

UC Berkeley

UC Berkeley Previously Published Works

Title

Systematic engineering for production of anti-aging sunscreen compound in *Pseudomonas putida*

Permalink

<https://escholarship.org/uc/item/38g6r8jw>

Authors

Yunus, Ian S
Hudson, Graham A
Chen, Yan
[et al.](#)

Publication Date

2024-06-01

DOI

10.1016/j.ymben.2024.06.001

Copyright Information

This work is made available under the terms of a Creative Commons Attribution License, available at <https://creativecommons.org/licenses/by/4.0/>

Peer reviewed

1 **Systematic engineering for production of anti-aging sunscreen compound in**
2 ***Pseudomonas putida***

3
4 Ian S. Yunus^{1,2,*}, Graham A. Hudson^{1,2,3}, Yan Chen^{1,2}, Jennifer W. Gin^{1,2}, Joonhoon Kim^{1,4},
5 Edward E. K. Baidoo^{1,2}, Christopher J. Petzold^{1,2}, Paul D. Adams^{1,5}, Blake A. Simmons^{1,2},
6 Aindrila Mukhopadhyay^{1,2}, Jay D. Keasling^{1,2,3,6,7,8}, and Taek Soon Lee^{1,2,*}

7
8 ¹Joint BioEnergy Institute, 5885 Hollis Street, Emeryville, CA, USA

9 ²Biological Systems & Engineering Division, Lawrence Berkeley National Laboratory, Berkeley,
10 CA, USA

11 ³California Institute of Quantitative Biosciences (QB3), University of California, Berkeley, CA, USA

12 ⁴Energy Processes & Materials Division, Pacific Northwest National Laboratory, Richland, WA,
13 USA

14 ⁵Molecular Biophysics & Integrated Bioimaging Division, Lawrence Berkeley National Laboratory,
15 Berkeley, CA, USA

16 ⁶Department of Chemical & Biomolecular Engineering, University of California, Berkeley, CA,
17 USA.

18 ⁷Department of Bioengineering, University of California, Berkeley, CA, USA.

19 ⁸Center for Biosustainability, Danish Technical University, Lyngby, Denmark

20
21 *Corresponding Authors, Joint BioEnergy Institute, 5885 Hollis Street, Emeryville, CA 94608,
22 USA.

23 E-mail addresses: tslee@lbl.gov (T. S. Lee). Tel: +1-510-495-2470. Fax: +1-510-495-2629;
24 iansofianyunus@gmail.com (I. S. Yunus).

25
26

27 **Abstract**

28 Sunscreen has been used for thousands of years to protect skin from ultraviolet radiation.
29 However, the use of modern commercial sunscreen containing oxybenzone, ZnO, and TiO₂ has
30 raised concerns due to their negative effects on human health and the environment. In this study,
31 we aim to establish an efficient microbial platform for production of shinorine, a UV light absorbing
32 compound with anti-aging properties. First, we methodically selected an appropriate host for
33 shinorine production by analyzing central carbon flux distribution data from prior studies alongside
34 predictions from genome-scale metabolic models (GEMs). We enhanced shinorine productivity

35 through CRISPRi-mediated downregulation and utilized shotgun proteomics to pinpoint potential
36 competing pathways. Simultaneously, we improved the shinorine biosynthetic pathway by refining
37 its design, optimizing promoter usage, and altering the strength of ribosome binding sites. Finally,
38 we conducted amino acid feeding experiments under various conditions to identify the key limiting
39 factors in shinorine production. The study combines meta-analysis of ¹³C-metabolic flux analysis,
40 GEMs, synthetic biology, CRISPRi-mediated gene downregulation, and omics analysis to
41 improve shinorine production, demonstrating the potential of *Pseudomonas putida* KT2440 as
42 platform for shinorine production.

43

44 *Keywords: natural products, mycosporine-like amino acid (MAA), CRISPR interference*
45 *(CRISPRi), Pseudomonas, genome-scale model, proteomics*

46

47

48 **Highlights:**

- 49 • Meta-analysis of ¹³C-MFA and GEMs show *P. putida* to be an ideal host for shinorine
50 production.
- 51 • CRISPRi-mediated gene downregulation of PP_1444 improves shinorine production.
- 52 • Shinorine was produced at high titers and amino acid supplementation improved the
53 titer.
- 54 • Shinorine accumulates exclusively in the supernatant in *P. putida* cultures.

55

56 1. Introduction

57 Extended warm periods (Oliver et al., 2018), global warming (Johnson et al., 2022), and
58 excessive use of chemical sunscreens (Roberto et al., 2008) have been linked to world-wide coral
59 bleaching. Due to concerns about their adverse effects on both human health and the
60 environment, several countries and regions have prohibited the use of commercial sunscreens
61 containing oxybenzone, octinoxate, ZnO, and TiO₂. This has led to a rising demand for
62 sunscreens derived from environmentally friendly sources. Shinorine, a mycosporine-like amino
63 acid (MAA) typically produced by red algae *Porphyra umbilicalis*, has been used as an active
64 ingredient in commercial sunscreen products (e.g., Helioguard™ 365, Helionori®). Shinorine has
65 also demonstrated additional benefits including anti-aging properties, antioxidant effects,
66 promotion of wound healing, and inhibition of UV radiation-induced skin inflammation (Choi et al.,
67 2015; Hartmann et al., 2015; Orfanoudaki et al., 2020; Suh et al., 2014; Torres et al., 2018). The
68 yield of shinorine from *P. umbilicalis*, however, is low (3.27 mg/g cell dry weight) (Becker et al.,
69 2016), and its production suffers from the slow growth of *P. umbilicalis*. With the continuous rise
70 in global demand for sunscreen, the bioproduction of shinorine in a fast-growing microbe emerges
71 as an attractive solution.

72 To meet the growing demand of shinorine, various host organisms, including
73 *Saccharomyces cerevisiae* (Jin et al., 2021; Kim et al., 2023, 2022; Park et al., 2019),
74 *Corynebacterium glutamicum* (Tsuge et al., 2018), *Synechocystis* sp. PCC 6803 (Yang et al.,
75 2018), *Streptomyces avermitilis* (Miyamoto et al., 2014), and *Yarrowia lipolytica* (Jin et al., 2023),
76 have been genetically engineered for shinorine production. Most metabolic engineering efforts
77 within the aforementioned host organisms, however, have primarily focused on coupling the
78 shinorine production pathway with the xylose utilization pathway to enhance the xylulose 5-
79 phosphate pool (Jin et al., 2023; Kim et al., 2023, 2022; Park et al., 2019). While this approach
80 has been proven to improve the shinorine titers, challenges persist. The highest shinorine
81 productivity (12.75 mg/L/h) and yield (36 mg/g total sugar) were achieved in *Saccharomyces*
82 *cerevisiae* in a fed-batch bioreactor (Kim et al., 2023). However, supplying sugar mixtures (e.g.,
83 hexoses and pentoses) into cultures introduces complexities to production experiments (Park et
84 al., 2019), as microbial hosts typically exhibit a preference for hexose (e.g., glucose) consumption
85 over pentose (e.g., xylose) (Aidelberg et al., 2014; Dvořák and de Lorenzo, 2018; Yan Wang et
86 al., 2019). Additionally, a large portion of shinorine produced from *S. cerevisiae* and *Y. lipolytica*
87 tends to accumulate within the cells (Jin et al., 2023; Kim et al., 2023), complicating extraction
88 and purification.

89 In this study, we methodically selected an appropriate host for shinorine production by
90 analyzing central carbon flux distribution data from prior studies alongside predictions from
91 genome-scale metabolic models (GEMs). We identified *Pseudomonas putida* KT2440 as a
92 promising host for shinorine production. We then developed synthetic biology tools for use in this
93 microbe and heterologously expressed shinorine biosynthetic gene cluster (BGC) from *Anabaena*
94 *variabilis* ATCC 29413. We enhanced shinorine productivity through CRISPRi-mediated
95 downregulation of potential competing pathways. Simultaneously, we improved the shinorine
96 biosynthetic pathway by refining its design, optimizing promoter usage, and altering the strength
97 of ribosome binding sites. Finally, we conducted amino acid feeding experiments under various
98 conditions and utilized shotgun proteomics to identify the limiting factors in shinorine production.
99 Altogether, our study provides a comprehensive framework for engineering *P. putida* KT2440 as
100 an efficient chassis for shinorine production.

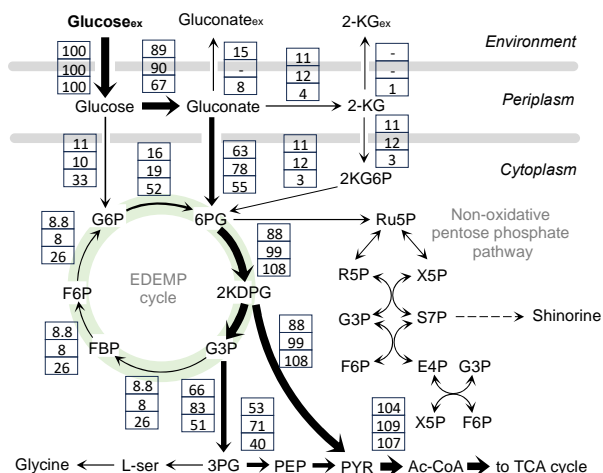
101

102 **2. Results and Discussion**

103 **2.1 Selection of *P. putida* KT2440 as a suitable host for shinorine production**

104 To select a suitable host for shinorine production, we reviewed published metabolic flux
105 distribution from commonly used biomanufacturing hosts with available ¹³C-metabolic flux
106 analysis (MFA) data (Figure 1, Supplementary Table S1) alongside predictions from genome-
107 scale metabolic models (GEMs) (Supplementary Table S2). We primarily focused on analyzing
108 fluxes directed towards 6-phosphogluconate (6PG) as this intermediary metabolite plays
109 important roles in the shinorine biosynthetic pathway. 6PG functions as an intermediate molecule
110 in both the pentose-phosphate and the Entner-Doudoroff pathways. In the pentose-phosphate
111 pathway, 6PG undergoes decarboxylation to produce ribulose 5-phosphate (Ru5P), which is
112 further metabolized into ribose 5-phosphate (R5P) and xylulose 5-phosphate (X5P) by ribulose-
113 5-phosphate epimerase. While R5P serves as a fundamental building block for nucleic acid
114 synthesis, X5P is converted by a transketolase to glyceraldehyde 3-phosphate (G3P) and
115 sedoheptulose 7-phosphate (S7P), acting as a precursor for shinorine biosynthesis. G3P is
116 converted to 3-phosphoglycerate (3PG) through either glycolysis (the Embden-Meyerhof-Parnas
117 (EMP) pathway) or the Entner-Doudoroff pathway. 3PG is used for the biosynthesis of *L*-serine
118 and glycine, essential amino acids incorporated into the shinorine biosynthetic pathway.

119



120
 121 Figure 1. Metabolic flux distribution of glucose-fed *Pseudomonas putida* KT2440. All values in boxes are given as
 122 relative fluxes normalized to the specific glucose uptake rate. Data are referenced from three primary studies:
 123 (Kukurugya et al., 2019) (top), (Nikel et al., 2015) (middle), and (Kohlstedt and Wittmann, 2019) (bottom). Arrow widths
 124 are proportional to the average of the three values. Abbreviations: G6P, glucose 6-phosphate; F6P, fructose 6-
 125 phosphate; FBP, fructose-1,6-biphosphate; DHAP, dihydroxyacetone phosphate; 6PG, 6-phosphogluconate; KDPG,
 126 2-keto-3-deoxy-6-phosphogluconate; Ru5P, ribulose 5-phosphate; R5P, ribose 5-phosphate; X5P, xylulose 5-
 127 phosphate; S7P, sedoheptulose 7-phosphate; E4P, erythrose 4-phosphate; G3P, glyceraldehyde 3-phosphate; 3PG,
 128 3-phosphoglycerate; PEP, phosphoenolpyruvate; Ac-CoA, acetyl-coenzyme A; L-ser, L-serine; TCA, tricarboxylic acid;
 129 PYR, pyruvate

130
 131 In most organisms, except for *P. putida* KT2440 and *Bacillus megatarium* QM B1551,
 132 glucose is directly phosphorylated by glucokinase, producing glucose 6-phosphate (G6P) (Fig. 1,
 133 Supplementary Figure S1). G6P can be either isomerized to fructose 6-phosphate (F6P) within
 134 the glycolytic pathway or undergo oxidation to form 6PG through the oxidative pentose phosphate
 135 pathway. The carbon flux distribution from G6P to F6P or G6P to 6PG, as determined through
 136 ¹³C metabolic flux analysis (¹³C-MFA), varies among different microorganisms and is influenced
 137 by factors such as fermentation conditions and genetic variations (Supplementary Table S1).
 138 Nonetheless, meta-analysis of ¹³C-MFA and predictions from GEMs (Supplementary Table S2)
 139 reveal that only a few microbes can allocate more than 50% of their carbon flux towards 6PG.

140 *Zymomonas mobilis* converts approximately 99% of its glucose supply to 6PG
 141 (Supplementary Table S1). However, the oxidative branch of the pentose phosphate pathway in
 142 *Z. mobilis* appears inactive as *Z. mobilis* lacks 6PG dehydrogenase enzyme (De Graaf et al.,
 143 1999; Jacobson et al., 2019). Instead of using the oxidative branch of the pentose phosphate
 144 pathway, *Z. mobilis* uses the non-oxidative branch and converts F6P to R5P and S7P through a
 145 series of enzymatic reactions. Only 0.8% carbon flux is distributed from G6P to F6P, leaving a
 146 very small pool of F6P for S7P synthesis. On the other hand, *in silico* metabolic network analysis

147 of *Rhodospiridium toruloides* reveals that glucose-fed *R. toruloides* allocates 89.7% of its carbon
148 flux towards 6PG, creating a significant pool of S7P in the non-oxidative pentose phosphate
149 pathway (Bommareddy et al., 2015). *R. toruloides* is also an attractive host for industrial scale
150 production of many chemical compounds (Liu et al., 2023, 2020; Schultz et al., 2022; Wehrs et
151 al., 2019). It can readily co-consume C5 and C6 sugars derived from lignocellulosic biomass and
152 grows to very high cell density. However, engineering *R. toruloides* has been challenging (Wen
153 et al., 2020) with only a few synthetic biology tools available (Brink et al., 2023).

154 *P. putida* KT2440 exhibits a distinctive central carbon metabolism (Fig. 1). In this microbe,
155 glucose can be phosphorylated to G6P in the cytoplasm through direct phosphorylation, or it can
156 undergo oxidation to gluconate catalyzed by glucose dehydrogenase in the periplasm.
157 Subsequently, gluconate can follow one of two routes: it can be phosphorylated to 6PG by
158 gluconokinase in the cytoplasm or oxidized to 2-ketogluconate (2-KG) in the periplasm. The latter
159 compound, 2-KG, is then transported into the cytoplasm and converted to 2-keto-6-
160 phosphogluconate (2K6PG) by 2-KG kinase, which is further reduced to 6PG by 2K6PG
161 reductase. While most glucose is oxidized to gluconate, regardless of the initial step in glucose
162 processing, these pathways converge into the production of 6PG. Furthermore, in contrast to
163 other microorganisms, *P. putida* KT2440 favors the conversion of F6P to 6PG rather than the
164 reverse reaction. As a result, *P. putida* KT2440 converts over 90% of its glucose supply to 6PG,
165 creating a substantial pool of 6PG for the biosynthesis of Ru5P and S7P in the non-oxidative
166 pentose-phosphate pathway. In addition, genome editing and synthetic biology tools for *P. putida*
167 KT2440 have been widely available and well characterized (Nikel and de Lorenzo, 2018). This
168 unique metabolic trait positions *P. putida* KT2440 as a promising host for shinorine production.

169

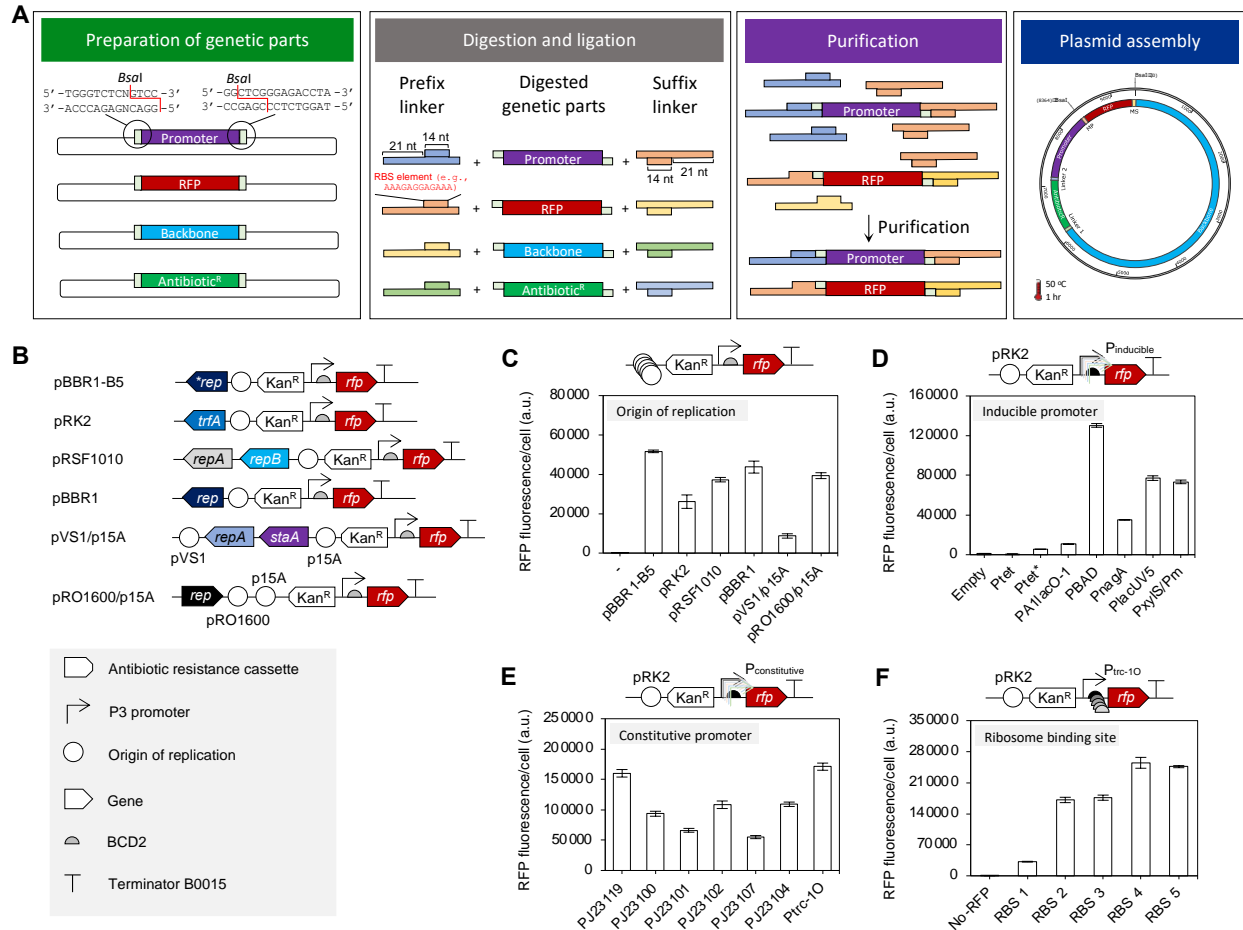
170

171 **2.2 Development of synthetic biology tools for gene expression in *P. putida* KT2440**

172 To establish the shinorine biosynthetic pathway, we began by first developing a modular
173 plasmid assembly tool for use in *P. putida* KT2440 (Fig. 2A). Here, we used Biopart Assembly
174 Standard for Idempotent Cloning (BASIC) (Storch et al., 2015) plasmid assembly method to allow
175 multipart DNA assembly using standard reusable parts in a single pot assembly reaction. The
176 resulting expression plasmids were then used to assess the functionality of genetic elements,
177 such as promoters and ribosome binding sites. The primary objective of this effort was not an
178 exhaustive characterization of the genetic elements but rather an investigation of the performance
179 of the expression plasmid and individual genetic elements employed in this study.

180 Six plasmids (pBBR1, pBBR1-B5, pRK2, pRSF1010, pRO1600/p15a, and pVS1/p15a)
181 with distinct backbones, copy numbers, and origin of replications were constructed and
182 characterized (Fig. 2B) by measuring the fluorescence intensity of a red fluorescent protein (RFP).
183 The plasmids selected for construction offer diverse features. First, pBBR1, isolated from
184 *Bordetella bronchiseptica* S87 (Antoine and Loch, 1992), is a broad host range plasmid origin
185 commonly used for gene expression in metabolic engineering studies of *P. putida* (Niu et al.,
186 2020; Tiso et al., 2016; X. Wang et al., 2022; Wohlers et al., 2021). Although generally considered
187 a low- to medium-copy plasmid with 30 copies per chromosome (Cook et al., 2018), the copy
188 number of pBBR1 can be altered by mutations in the *rep* gene (Tao et al., 2005). Second, pBBR1-
189 B5, a variant of pBBR1 plasmid with an early stop codon in the *rep* gene, exhibits around 70
190 copies per chromosome, a higher copy number than the original pBBR1 plasmid. Third, the
191 plasmid pRK2 is a member of the IncP incompatibility group and requires an origin of replication
192 and a replication initiation protein encoded by *trfA* to function. It has been shown to be stably
193 maintained in *P. putida* and has been measured to be a low-copy plasmid in *Escherichia coli* (
194 De Bernardez and Dhurjati, 1987) and has around 30 copies per chromosome in *P. putida* (Cook
195 et al., 2018). Fourth, RSF1010 is a high-copy broad host range plasmid with 130 copies per
196 chromosome and is a part of the IncQ incompatibility group plasmid. It has been routinely used
197 for gene expression in *P. putida* (Aparicio et al., 2019). Lastly, pRO1600 (Farinha and Kropinski,
198 1990) and pVS1 (Itoh and Haas, 1985) are plasmids isolated from *Pseudomonas* species,
199 requiring host-specific origins (e.g., p15a, that replicates in *E. coli*) to generate shuttle vectors for
200 *P. putida*. In this study, plasmid characterization reveals that pBBR1-B5 shows the highest RFP
201 fluorescence level, followed by pBBR1 > pRSF1010 = pRO1600/p15a > pRK2 > pVS1/p15a
202 plasmids (Figure 2C).

203



204

205 Figure 2. Development of genetic tools for gene expression in *Pseudomonas putida* KT2440. (A) Modular cloning
 206 assembly method as described in a previously published work (Storch et al., 2015). Genetic parts were cloned into a
 207 pJET1.2 blunt DNA plasmid. Subsequently, these parts were digested with *BsaI* restriction enzyme and ligated with
 208 prefix and suffix linkers, followed by separation and purification using magnetic beads. Finally, purified genetic parts
 209 and linkers were assembled in one-pot reaction at 50 °C for 1 h. (B) Schematic diagrams of plasmids with different
 210 backbones. RFP fluorescence levels measured across various plasmid backbones (C), under different inducible
 211 promoters (D), constitutive promoters (E), and ribosome binding site sequences (F). Cultures were grown in 5 mL of
 212 M9 minimal medium. RFP fluorescence was measured using a flow cytometer at 48 hr post-inoculation. Inducer was
 213 added at 0 h. Error bars represent the standard deviation of three biological replicates.

214

215 Given its medium-range RFP fluorescence, plasmid pRK2 was then selected as the
 216 plasmid backbone for the characterization of different inducible (Figure 2D) and constitutive
 217 (Figure 2E) promoters. Seven different inducible promoters (P_{tet} (Cook et al., 2018), P_{tet^*} (Tian et
 218 al., 2019), $P_{A1lacO-1}$ (Liu et al., 2019), P_{BAD} (Calero et al., 2016), P_{NagA} (Hüsken et al., 2001), P_{lacUV5}
 219 (Noel Jr. and Reznikoff, 2000), and $P_{XylIS/Pm}$ (Calero et al., 2016)), six constitutive promoters
 220 (Anderson et al., 2010) with varying strength (P_{J23119} , P_{J23100} , P_{J23101} , P_{J23102} , P_{J23107} , P_{J23104}), and
 221 P_{trc1-O} (Bagdasarian et al., 1983; Calero et al., 2016) (without a LacI repressor) were characterized.

222 P_{tet} and $P_{A1lacO-1}$ promoters exhibited a high basal fluorescence level (Supplementary Figure S2)
223 compared to other promoters. Among the inducible promoters, P_{BAD} , the arabinose-inducible
224 promoter, showed the highest RFP fluorescence level. Meanwhile, under the conditions tested,
225 the constitutive promoter P_{trc-10} was the strongest promoter among all evaluated promoters.

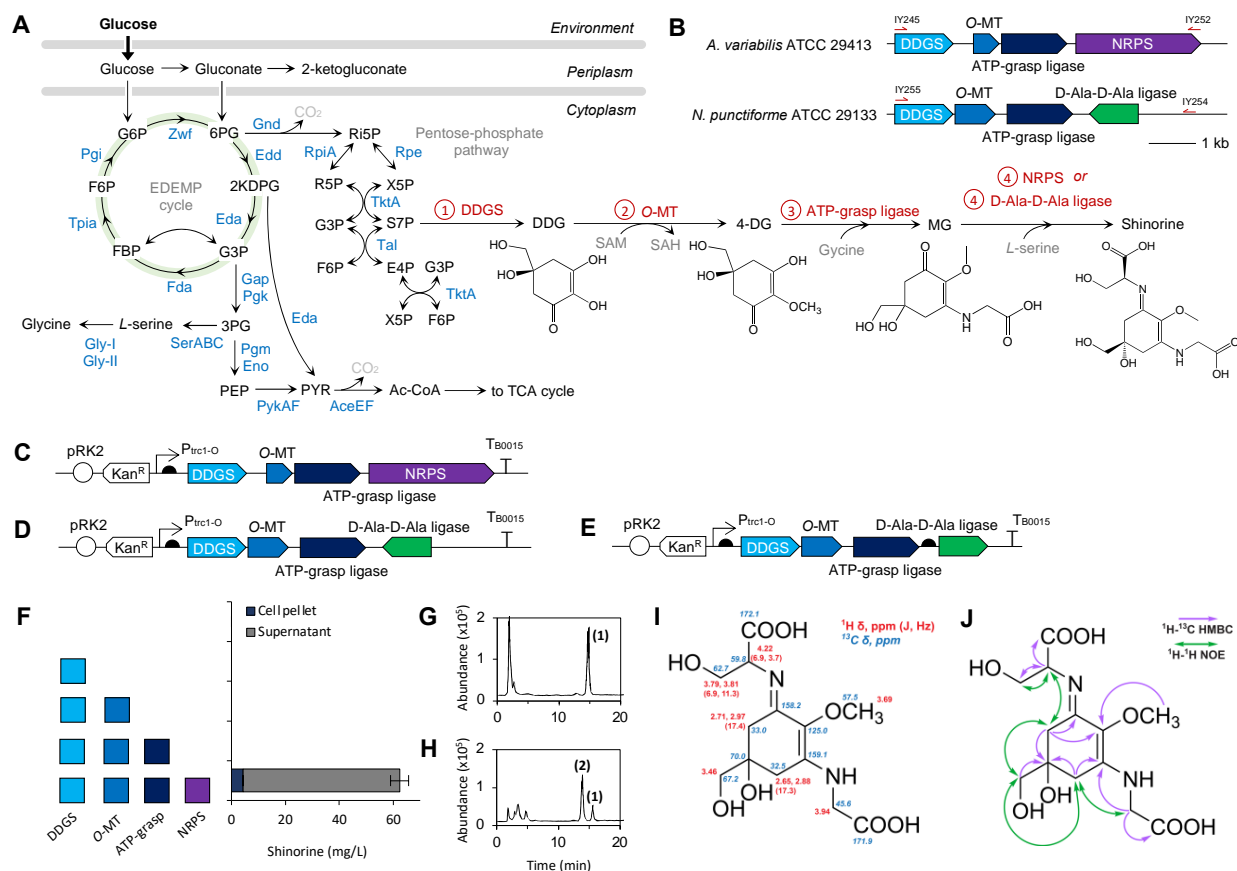
226 Lastly, we characterized ribosome binding site (RBS) elements tailored for application in
227 *P. putida* KT2440. The use of RBSs with varying strengths has been employed in metabolic
228 engineering studies, proving to be a useful strategy for pathway optimization. Despite its
229 significance, RBS characterization in *P. putida* has only been described in a few studies. First,
230 Elmore and colleagues characterized ten different RBS elements by mutating four nucleotides
231 within the core RBS sequence (Elmore et al., 2017). In combination with different promoters, the
232 RBS they generated exhibited up to 7-fold differences in the expression levels of mNeonGreen.
233 In another study, Damalas and colleagues leveraged the RBS calculator (Salis, 2011) to
234 computationally predict six RBS sequences. These RBS sequences, compatible with The
235 Standard European Vector Architecture (SEVA) platform or the BioBrick assembly, expanded the
236 synthetic biology toolkit in *P. putida* (Damalas et al., 2020). In the following study, Aparicio and
237 colleagues employed recombineering techniques to generate a library of 33 RBS variants
238 (Aparicio et al., 2020). Unique to those studies, here, we embedded an RBS element into a prefix
239 linker (Fig. 2A) to enable the flexible placement of RBS linker upstream of the coding sequence
240 of any gene of interest. We selected three RBS sequences from BioBrick (Shetty et al., 2008)
241 (RBS1; ATCACACAGGAC (Bba_B0033), RBS2; AAAGAGGGGAAA (Bba_B0064), and RBS3;
242 AAAGAGGAGAAA (Bba_B0034)), a Shine-Dalgarno *E. coli* consensus (RBS4;
243 ATCACAAGGAGG), and an anti-Shine-Dalgarno complementary sequence (RBS5:
244 ATTAGTGGAGGT). These RBS linkers have previously been characterized in *E. coli* (Storch et
245 al., 2015), demonstrating a wide range of fluorescent protein expression levels. However, these
246 RBS linkers are yet to be characterized in *P. putida*.

247 Evaluation of the RBS linkers in *P. putida* revealed that the selected ribosome binding
248 sites exhibited varying strengths, low (RBS 1), medium (RBS 2 and RBS 3), and high (RBS 4 and
249 5) with an 8-fold difference between the weakest and strongest RBS (Fig. 2F). We anticipate that
250 when combined with different promoters, these selected RBS elements will provide a diverse
251 array of options for fine-tuning and optimizing biosynthetic pathways in future studies. All in all,
252 the characterization of these genetic elements, alongside the introduction of linker-based modular
253 cloning assembly method tailored for *P. putida* KT2440, heralds an expansion of the synthetic
254 biology toolkit for this organism. Such progress paves the path for more efficient and customized
255 metabolic engineering efforts in *P. putida*.

256
257
258
259
260
261
262
263
264
265
266
267
268
269
270
271
272
273
274
275

2.3 Shinorine production in *Pseudomonas putida* KT2440

After evaluating the performance and functionality of plasmid backbones, promoters, and ribosome binding sites in *P. putida* KT2440, we began constructing the shinorine biosynthetic pathway (Fig. 3A). The shinorine biosynthetic gene cluster (BGC) has been identified in various microorganisms, including *Anabaena variabilis* ATCC 29413 (Emily P Balskus and Walsh, 2010), *Nostoc punctiforme* ATCC 29133/PCC 73102 (Qunjie and Ferran, 2011), *Actinosynnema mirum* DSM 43827 (Miyamoto et al., 2014), *Chlorogloeopsis fritschii* PCC 6912 (Llewellyn et al., 2020; Portwich and Garcia-Pichel, 2003), and *Fischerella* sp. PCC 9339 (Yang et al., 2018). In this study, we selected the shinorine biosynthetic pathway from *Anabaena variabilis* ATCC 29413 and *Nostoc punctiforme* ATCC 29133 as the two BGCs have been used for shinorine biosynthesis in various organisms (Jin et al., 2023; Kim et al., 2023; Park et al., 2019). S7P, an intermediate metabolite of the pentose phosphate pathway, is converted into shinorine through a series of four enzymatic steps. Firstly, S7P undergoes transformation into 4-deoxygadusol (4-DG) by 2-demethyl 4-deoxygadusol synthase (DDGS) and O-methyltransferase (O-MT). Subsequently, glycine is conjugated to 4-DG by ATP-grasp ligase to form mycosporine-glycine (MG). Finally, a serine moiety is attached to MG by a nonribosomal peptide synthetase (NRPS)-like enzyme in *Anabaena variabilis* ATCC 29413 or by a D-Ala-D-Ala ligase in *Nostoc punctiforme* ATCC 29133 (Fig. 3A,B).



276
 277 Figure 3. Production experiment of shinorine in engineered *P. putida* KT2440 and confirmation by nuclear magnetic
 278 resonance (NMR) spectroscopy. (A) Schematic diagram of *P. putida* KT2440 central carbon metabolism and shinorine
 279 biosynthetic pathway. The initial biosynthetic step involves the synthesis of desmethyl 4-deoxygadusol (DDG) through
 280 sedoheptulose 7-phosphate (Balskus and Walsh, 2010; Pope et al., 2015). Desmethyl-4-deoxygadusol synthase
 281 (DDGS) catalyzes the production of DDG. Subsequently, *O*-methyltransferase (*O*-MT) transforms DDG to 4-
 282 deoxygadusol (4-DG). 4-DG incorporates glycine through an ATP-grasp ligase to yield mycosporine-glycine (MG). In
 283 the final step, MG is converted to shinorine by a non-ribosomal peptide synthetase (NRPS)-like enzyme (Balskus and
 284 Walsh, 2010; Portwich and Garcia-Pichel, 2003), which encompasses adenylation, thiolation, and thioesterase domains
 285 or by a D-Ala-D-Ala ligase. The adenylation domain plays a crucial role in attaching serine to the C1 position of
 286 mycosporine-glycine, generating shinorine. (B) Shinorine biosynthetic gene cluster (BGC) from *Anabaena variabilis*
 287 ATCC 29413 and *Nostoc punctiforme* ATCC 29133. Primers are indicated by red arrows. (C) Schematic diagram of
 288 plasmid pLY456 used for expression of shinorine BGC from *A. variabilis* ATCC 29413. This plasmid was used for
 289 production experiments in Fig. 3F. (D) Plasmid used for expression of shinorine BGC from *N. punctiforme* ATCC 29133.
 290 (E) Variation of plasmid shown in Fig. 3D with the introduction of a foreign RBS upstream the D-Ala-D-Ala ligase coding
 291 sequence. (F) Production of shinorine in *P. putida* KT2440 strains. Chromatogram obtained from *P. putida* (G) and
 292 extracted Helioguard™ (H). (I) Assigned ¹H and ¹³C resonances for purified shinorine. (J) Correlations (¹H-¹H NOESY
 293 and ¹H-¹³C HMBC) used to unambiguously assign all resonances for purified shinorine. *P. putida* KT2440 were grown
 294 in 5 mL M9 medium, and samples were extracted at 48 h. Error bars represent standard deviations from three biological
 295 replicates. SAM, S-adenosyl-L-methionine; SAH, S-adenosylhomocysteine. Other abbreviations are shown in Figure 1
 296 caption.

297 To synthesize shinorine in *P. putida* KT2440, we began by amplifying the whole shinorine
298 BGC from *A. variabilis* ATCC 29413 (MIBiG Accession Number: BGC0000427) and *N.*
299 *punctiforme* ATCC 29133 (Balskus and Walsh, 2010; Qunjie and Ferran, 2011), keeping the
300 intergenic regions unaltered. The amplified gene clusters were subsequently cloned into an RK-
301 based vector under the control of a strong constitutive P_{trc1-O} promoter (Fig. 3C,D). As the gene
302 encoding D-Ala-D-Ala ligase appeared to be transcribed in the antisense direction, we also
303 created another plasmid variant where we introduced a foreign RBS and changed the orientation
304 of the gene (Fig. 3E). Despite several attempts, the production of shinorine in *P. putida* KT2440
305 could only be detected from the heterologous expression of shinorine BGC from *A. variabilis*
306 ATCC 291413, yielding approximately 60 mg/L shinorine at 48 hr (Fig. 3F), with over 80% of
307 shinorine accumulating in the supernatant.

308 The chromatographic analysis of the samples (Fig. 3G) showed that the shinorine peak
309 (1) co-eluted with the shinorine peak obtained from the reference Helioguard™ standard (Fig.
310 3H). The accuracy of the mass spectrum was confirmed through LC-MS/MS (Supplementary
311 Figure S3) and the results agreed with those previously reported (Kim et al., 2022). To further
312 validate the chemical structure of shinorine, we purified the extract from a 1-L liquid culture and
313 subjected it to nuclear magnetic resonance (NMR) spectroscopy. Correlations obtained via ^1H - ^1H
314 COSY, ^1H - ^1H NOESY, ^1H - ^{13}C HSQC and ^1H - ^{13}C HMBC enabled the unambiguous assignment of
315 all ^1H and ^{13}C resonances (Figure 3I, J and Supplementary Table S3). Observed resonances and
316 assignments thereof were highly consistent with previous NMR data reported for shinorine
317 (Miyamoto et al., 2014) (Supplementary Figures S4-S10). To our knowledge, this is the first report
318 of shinorine production in *P. putida* KT2440.

319

320 **2.4 Improvement of shinorine production titer by CRISPRi-mediated gene** 321 **downregulation**

322 To further improve the shinorine titer, we employed CRISPRi-mediated gene
323 downregulation to suppress competing metabolic pathways and redirect carbon flux towards
324 shinorine production. The use of CRISPRi holds the potential to improve the yield of desired
325 metabolites by selectively repressing the expression of specific genes in metabolic pathways.
326 This approach has proven successful in improving the production of various compounds, including
327 isoprenol (Tian et al., 2019; Wang et al., 2022), free fatty acids (Fang et al., 2021), propane
328 (Yunus et al., 2022), fatty alcohols (Kaczmarzyk et al., 2018), indigoidine (Banerjee et al., 2020),
329 and many others (Zhao et al., 2021). In this study, we applied CRISPRi to downregulate a set of
330 twenty-one genes involved in the central carbon metabolism and biosynthesis of *L*-serine and

331 glycine, two amino acids critical to the shinatorine biosynthetic pathway (Fig. 4A). Catalytically
332 inactive Cas9 protein was expressed in RSF1010 plasmid under the control of salicylic acid-
333 inducible promoter (P_{nagA}) and the single guide RNA (sgRNA) was placed under the constitutive
334 promoter P_{J23119} (Fig. 4B). This plasmid was coexpressed with the shinatorine-producing RK2
335 plasmid.

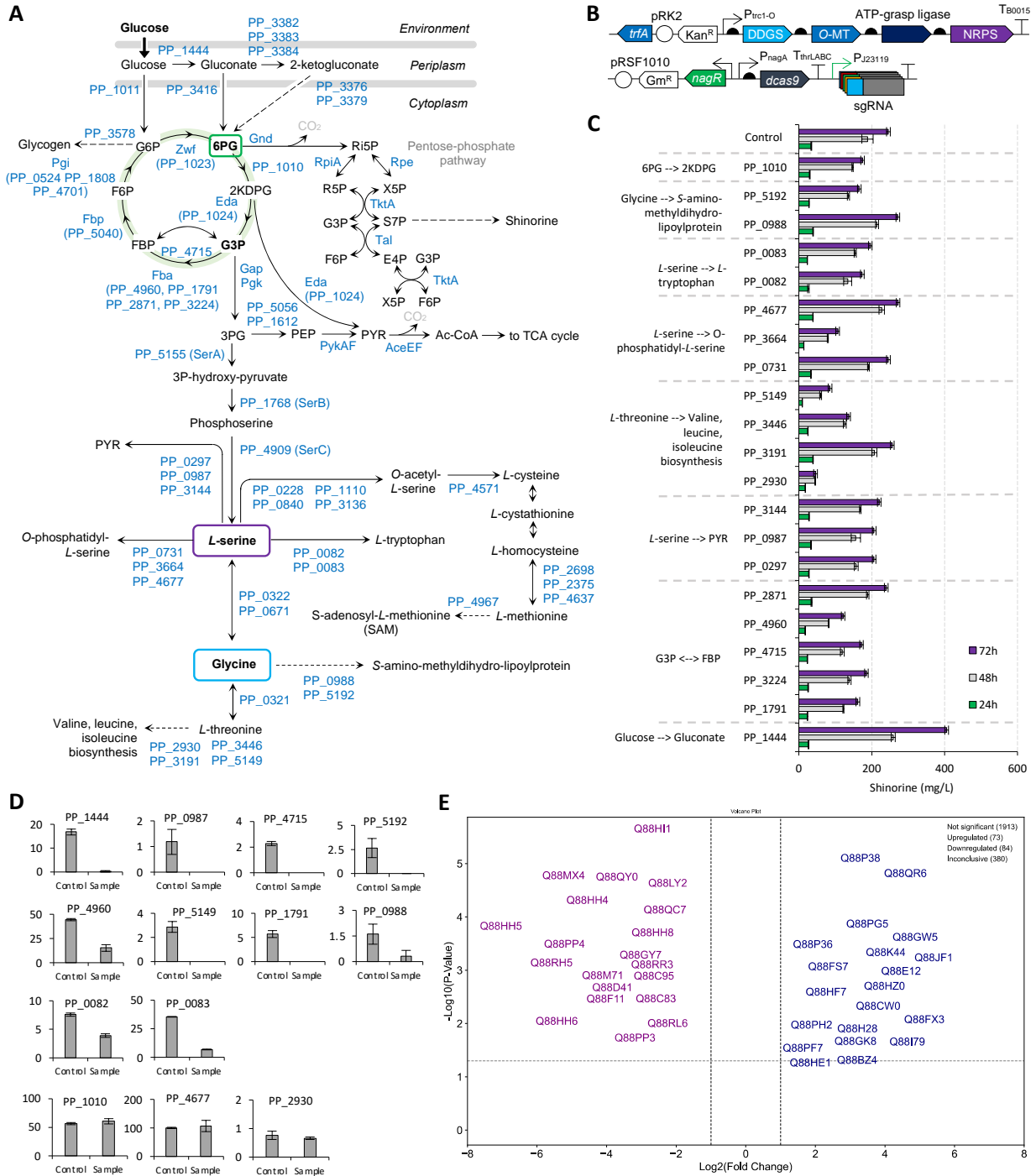
336 Our findings demonstrated that knocking down the PP_1444 gene led to a significant
337 increase in the shinatorine titer. The *P. putida* KT2440 strain with downregulated PP_1444
338 produced approximately 400 mg/L shinatorine in 72 hr, a 160% increase compared to the control
339 strain (i.e., a strain with a nontarget sgRNA) (Fig. 4C). It is worth noting that the titer of the control
340 strain shown here is approximately 3-fold higher at 48 hr compared to the strain shown in Fig. 3C.
341 The presence of a CRISPRi plasmid appeared to influence the expression levels of DDGS, O-
342 MT, ATP-grasp ligase, and NRPS (Supplementary Fig. S11). These changes might also be
343 attributed to the heightened expression of the *aph* gene (Supplementary Fig. S12B), which may
344 suggest that the copy number of the RK2 plasmid was altered in the presence of a second
345 plasmid.

346 PP_1444 encodes quinoprotein glucose dehydrogenase, the enzyme responsible for the
347 conversion of glucose to gluconate. In previous studies, it was observed that *P. putida* KT2440
348 tends to accumulate gluconate and 2-ketogluconate, and the accumulation of these two
349 compounds is effectively eliminated by knocking out PP_1444 (Teresa et al., 2007).
350 Interestingly, the knockout of PP_1444 has been associated with a growth defect in prior studies
351 (Bentley et al., 2020). However, in our study, we did not observe any growth defects
352 (Supplementary Fig. S13A). This discrepancy is likely attributable to the partial repression of
353 PP_1444 achieved by CRISPRi (Fig. 4D), resulting in a decrease rather than a complete
354 elimination of gluconate in both the supernatant and cell pellet fractions (Supplementary Fig.
355 S13B, C). The decrease in gluconate levels both in cell pellet and supernatant fraction might
356 indicate a potential redirection of carbon flux from glucose directly to the EDMP cycle.

357 To investigate the impact of PP_1444 downregulation on central carbon metabolism, we
358 performed metabolomics analyses on the control and PP_1444 strains at various sampling time
359 points (Supplementary Fig. S13D-H). Although no discernible difference in the G6P pool was
360 observed between the supernatant fractions of control (nontarget sgRNA) and PP_1444 strains
361 (in fact, G6P levels were lower in the cell pellet fraction of PP_1444 for the first 48 hr), we
362 consistently noted higher concentrations of 2/3PG and 6PG in both the supernatant and cell pellet
363 fractions of the PP_1444 strain (Supplementary Fig. S13D,H). This might indicate that knocking
364 down PP_1444 may enhance the availability of 6PG and 2/3PG, which can be beneficial for the

365 synthesis of glycine and *L*-serine. Interestingly, the S7P pool was lower in the cell pellet fraction
366 of the PP_1444 strain for the first 48 hr. One plausible explanation is that the lower S7P levels in
367 PP_1444 strain could be attributed to increased metabolic activity channeling S7P towards the
368 shinorine biosynthetic pathway, fueled by the increased availability of glycine and *L*-serine
369 substrates for shinorine biosynthesis. While these preliminary metabolomics findings offer
370 insights into the metabolic alterations induced by PP_1444 downregulation, a comprehensive
371 elucidation of the underlying mechanisms driving improvements of shinorine necessitates further
372 dedicated study.

373 As the downregulation of PP_1444 appeared to be the only instance resulting in an
374 increase in shinorine titer, we further investigated to verify the downregulation of other target
375 genes. Among the 21 targeted genes, we observed that 10 were indeed downregulated, 3
376 exhibited no downregulation, and 8 could not be verified as the proteins were undetectable in both
377 the sample and control strains (Fig. 4D). Of the three genes that were not downregulated
378 (PP_1010, PP_2930, and PP_4677), with the exception of PP_4677, their respective dCas9
379 expression levels were low (Supplementary Fig. S12C) although the expression levels of the
380 gentamicin selection markers were consistently maintained in these strains (Supplementary Fig.
381 S12A). Recognizing the significance of flux from 6PG to 2KDPG (Fig. 1) as the major competing
382 pathway for S7P synthesis, we designed additional sgRNAs targeting different regions within the
383 coding sequence of PP_1010. Despite these efforts, no improvement in shinorine titer was
384 observed. Sequencing analysis revealed mutations in the CRISPRi plasmid, resulting in a partial
385 deletion of the CRISPRi plasmid – although the plasmid was still intact when cloned in *E. coli*. We
386 hypothesized that since PP_1010 is an essential gene, as indicated by data retrieved from
387 fit.genomics.lbl.gov, knocking down the PP_1010 could be detrimental to growth. Therefore, only
388 *P. putida* KT2440 carrying the mutated CRISPRi plasmid (i.e., with no or low dCas9 expression)
389 could dominate the population. This hypothesis is in agreement with the low expression level of
390 dCas9 observed in our proteomics analysis. In the case of PP_4677, however, the dCas9
391 expression level was comparable to that of other strains. This leads us to speculate that the lack
392 of downregulation observed in PP_4677 may be attributed to the inefficiency of the designed
393 sgRNA of PP_4677. It underscores the importance of designing more effective sgRNAs to
394 achieve efficient gene regulation in future experiments.



396

397

398

399

400

401

Figure 4. CRISPRi gene downregulation for improved shinorine production. (A) Schematic diagram of genes involved in 6PG, G3P, L-serine, glycine, and S-adenosyl-L-methionine (SAM) metabolism. (B) Schematic diagram of plasmids used for expression of shinorine biosynthetic genes and CRISPRi-mediated gene downregulation. (C) Shinorine titer produced by different strains targeting 21 genes. (D) Relative expression levels (y-axis; $\times 10^6$) of target genes in the control vs sample. (E) Volcano plot depicting top 20 downregulated (purple) and upregulated (navy) genes in the

402 PP_1444 strain. The dashed horizontal line represents statistical significance threshold ($P \leq 0.05$). All strains were
403 cultivated in 5 mL M9 medium. Error bars represent standard deviation from three biological replicates.

404
405 Upon further investigation, in addition to PP_1444, we found that approximately 83 other
406 genes were unexpectedly significantly downregulated in the PP_1444 strain (Fig. 4E,
407 Supplementary Table S4). Among them, proteins involved in the metabolism of gluconate into 2-
408 ketogluconate and 6PG (Fig. 4A), such as Q88HH4, Q88HH5, and Q88HH6 (gluconate 2-
409 dehydrogenase, encoded by PP_3384, PP_3383, and PP_3382, respectively), as well as Q88HI1
410 (ketogluconate-6-P-reductase, encoded by PP_3376) and Q88HH8 (2-ketogluconate epimerase,
411 encoded by PP_3379), were downregulated. Phosphoglucomutase (Q88GY7, encoded by
412 PP_3578), an enzyme responsible for glycogen biosynthesis from G6P, also appeared to be
413 downregulated. This may redirect G6P pool for the synthesis of 6PG (Fig. 4A). Additionally, *L*-
414 serine dehydratase (Q88P66, encoded by PP_0987), which is involved in the conversion of *L*-
415 serine to pyruvate, was also downregulated. This might preserve *L*-serine pool for shinorine
416 biosynthesis. Interestingly, downregulating PP_0987 alone did not improve the shinorine titer (Fig.
417 4C). In addition to massive, unexpected gene downregulation, we found 73 genes were
418 upregulated in PP_1444 strain (Fig. 4E, Supplementary Table S5). For example, 5-
419 methyltetrahydropteroyltriglutamate-homocysteine methyltransferase (Q88JF1, encoded by
420 PP_2698), was upregulated by 28-fold. This enzyme may be responsible for maintaining *L*-
421 methionine synthesis used for biosynthesis of *S*-adenosyl-*L*-methionine (SAM), a methyl donor
422 for *O*-methyltransferase.

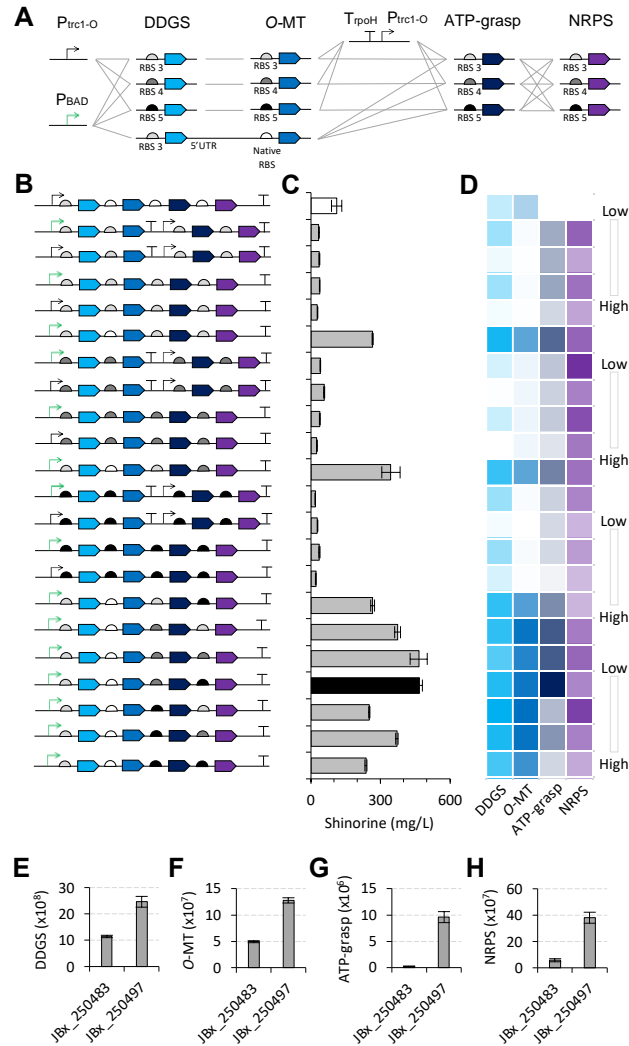
423 These results may demonstrate that the downregulation of PP_1444 not only reduces the
424 accumulation of gluconate but also has far-reaching effects on the expression of multiple genes
425 in *P. putida* KT2440. Many of the listed proteins appear to be involved in various metabolic
426 pathways, including amino acid and central carbon metabolism. Their direct roles in shinorine
427 production are not clear. While some of these gene expression changes align with our goal of
428 increasing shinorine production by redirecting carbon flux and preserving critical metabolites,
429 others remain unexplained and require further investigation. Nevertheless, these findings
430 highlight the potential of CRISPRi as a valuable tool for metabolic engineering and the production
431 of desired compounds in microbial hosts, offering promising avenues for further optimization and
432 enhancing the yield of shinorine and other valuable metabolites in biotechnological applications.

433
434 **2.5 Pathway optimization through refining promoter usage and altering the strength of**
435 **ribosome binding sites**

436 In tandem with CRISPRi-mediated gene downregulation approach, we sought to improve
437 the shinorine titer by refining the design of the genetic constructs, including optimizing promoter
438 usage, and altering the strength of ribosome binding sites. Previous studies have demonstrated
439 the effectiveness of adjusting RBS strength to enhance metabolite production (Jeschek et al.,
440 2017; Jones et al., 2015; Rao et al., 2024; Yunus et al., 2020; Yunus and Jones, 2018). However,
441 constructing plasmids for biosynthetic pathways involving multiple genes can be labor-intensive.
442 To streamline this process, we adopted a modular linker-based plasmid construction method
443 (Storch et al., 2015) to facilitate the creation of plasmid constructs with various RBSs, thereby
444 tuning the expression levels of proteins involved in the shinorine pathway (Fig. 5A).

445 By employing two distinct promoters (P_{BAD} and P_{trc1-O}) and restructuring the shinorine BGC
446 into either one or two transcriptional units, coupled with variations in RBSs, we successfully
447 assembled twenty-one different plasmids (Fig. 5B). This combinatorial approach led to a
448 significant increase in shinorine production, elevating it from 100 mg/L (Fig. 5C, JBx_250483,
449 represented by the white bar) to approximately 467 mg/L shinorine (Fig. 5C, JBx_250497,
450 represented by the black bar) within a 72-hr post inoculation.

451



452
 453 Figure 5. Improvement of shinatorine production by RBS optimization. (A) Illustration of combinatorial modular plasmid
 454 assembly consisting of promoters and genes assembled to different RBS. Two types of promoters and three different
 455 RBS elements were used. (B) Schematic diagram of twenty-one different shinatorine-producing plasmids. (C) Shinatorine
 456 titers from strains carrying plasmid shown in Fig. 5B. White bar and black bar charts represent JBx_250483 and
 457 JBx_250497 strain, respectively. (D) Heatmap of shotgun proteomics analysis of DDGS, O-MT, ATP-grasp ligase, and
 458 NRPS. Expression levels of DDGS (E), O-MT (F), ATP-grasp ligase (G), and NRPS (H) from the control strain
 459 (JBx_250483) vs the highest shinatorine producing strain (JBx_250497). Samples were grown in 5 mL of M9 minimal
 460 medium. Shinatorine was extracted from the whole liquid culture at 72 hr. Error bars represent standard deviations from
 461 three biological replicates.

462
 463 Our shotgun proteomics analysis revealed that manipulating promoters and RBSs proved
 464 to be a viable strategy for enhancing the expression levels of shinatorine pathway proteins (Fig.
 465 5D). The arabinose-inducible promoter P_{BAD} appeared to outperform the constitutive P_{trc1-O}
 466 promoter. Substituting the native RBS with foreign RBS sequences, except for the native O-MT

467 RBS, resulted in a significant increase in protein expression levels. By employing a foreign RBS,
468 we achieved substantial improvements in the expression levels of DDGS, O-MT, ATP-grasp
469 ligase, and NRPS in JBx_250497, with improvements of 2.1-fold, 2.6-fold, 40.5-fold, and 6.7-fold,
470 respectively, compared to the original strain (JBx_250483) (Fig. 5E-H).

471 To discern the enzyme(s) with the most significant impact on shinorine production, we
472 performed a multiple linear regression analysis. The Ordinary Least Squares (OLS) regression
473 results indicate that the expression levels of O-MT and ATP-grasp ligase carry considerable
474 statistical significance in predicting shinorine titer, whereas DDGS and NRPS do not appear to
475 have a significant effect in this model (Supplementary Table S6). This may imply that further
476 improvements in the expression levels of O-MT and ATP-grasp ligase could lead to a more
477 substantial increase in the shinorine titer. However, having robustly explored the available
478 permutations of RBS variations, we found that optimizing these two enzyme's expression levels
479 beyond a certain point did not yield significant improvements in shinorine production
480 (Supplementary Fig. S14). Therefore, while O-MT and ATP-grasp ligase play a crucial role in
481 predicting shinorine titer, there may be other factors or pathways that need to be considered for
482 further enhancement.

483

484 **2.6 Glycine and L-serine supplementation further improves shinorine production**

485 Following the successful implementation of CRISPRi-mediated gene downregulation and
486 the refinement of genetic constructs, we then combined the two strategies to further improve
487 shinorine production. We used the highest shinorine producing strain (JBx_250497) as the base
488 strain and co-transformed it with a CRISPRi plasmid harboring PP_1444 sgRNA or nontarget
489 sgRNA (Fig. 6A). The PP_1444 strain produced approximately 524 mg/L shinorine at 66 hr while
490 the control nontarget strain produced approximately 365 mg/L shinorine (Supplementary Fig.
491 S15). The glucose consumption profiles indicate that glucose was completely in both samples
492 after 42 hr. No significant growth and shinorine production were observed after 66 hr. These
493 results might imply that the glucose supply was limiting the shinorine production under the tested
494 condition.

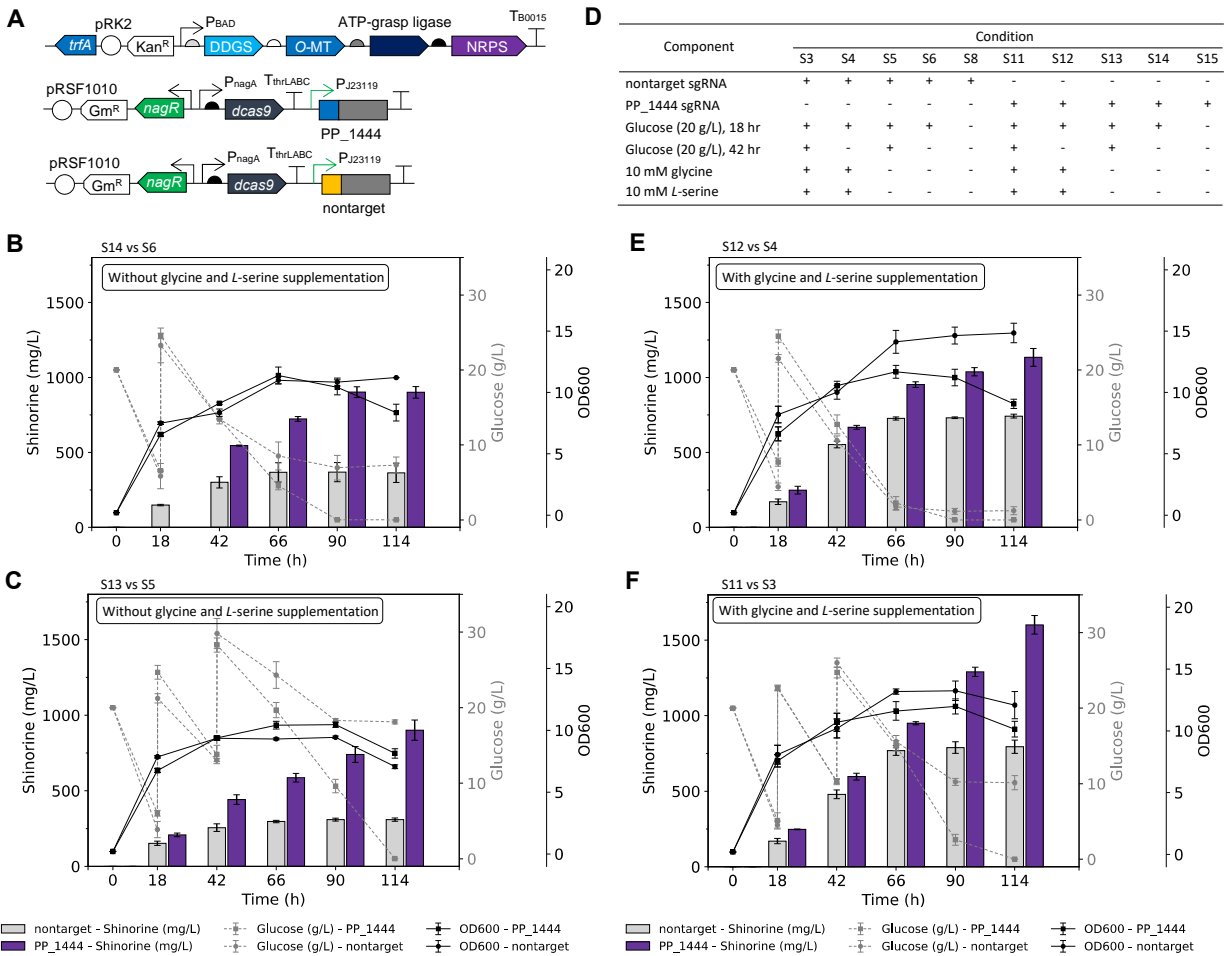
495 To increase the supply of glucose, we added 20 g/L of glucose at 18 hr. Upon the addition
496 of extra glucose, the PP_1444 strain produced approximately 723 mg/L of shinorine at 66 hr (Fig.
497 6B). The shinorine titer peaked at 902 mg/L at 90 hr. To explore if another glucose
498 supplementation would further improve the titer, we added an extra 20 g/L of glucose at 42 hr
499 (Fig. 6C) The additional glucose did not improve the final titer, indicating that another factor was
500 potentially limiting the shinorine production.

501 The shinorine biosynthetic pathway involves the incorporation of two amino acids, glycine
502 and *L*-serine. Glycine and *L*-serine are incorporated into the shinorine through specific enzymatic
503 reactions (Fig. 4A). The ATP-grasp ligase, a key enzyme in the shinorine biosynthetic pathway,
504 facilitates the incorporation of glycine into 4-deoxygadusol to form mycosporine-glycine, which is
505 a precursor of shinorine. Subsequently, an NRPS-like enzyme attaches a serine moiety to
506 mycosporine-glycine, resulting in the formation of shinorine. Considering the role of these amino
507 acids in shinorine biosynthesis, we hypothesized that their external supplementation could
508 potentially alleviate any metabolic bottleneck due to limited intracellular availability, thereby
509 enhancing the overall production of shinorine.

510 To test this hypothesis, we conducted a series of fermentation experiments of PP_1444
511 and nontarget strains (Fig. 6D) with supplementation of glycine and *L*-serine. The
512 supplementation of glycine and *L*-serine resulted in a marked increase in shinorine production,
513 both in the PP_1444 and nontarget strains (compared Fig. 6E and 6B). For the PP_1444 strain,
514 the shinorine titer increased sharply within the first 66 hr and then continued to steadily increase
515 up to 1,134 mg/L at 114 hr (Fig. 6E). Approximately 1.7 g/L of glucose remained in the liquid
516 cultures at 66 hr. To further improve the shinorine titer, we added an extra 20 g/L of glucose at 42
517 hr (Fig. 6F). Here, we observed a sharp increase of shinorine titer over 114 hr. The highest
518 shinorine titer of 1,601 mg/L was achieved at 114 hr from the PP_1444 strain, where the strain
519 completely consumed the glucose. In summary, without glycine and *L*-serine supplementation,
520 we achieved a final titer, productivity, and yield of 900 mg/L, 10 mg/L/h, and 22.5 mg/g glucose,
521 respectively. With the addition of glycine and *L*-serine, these metrics increased to 1,601 mg/L, 14
522 mg/L/h, and 26 – 28.35 mg/g glucose.

523 While these results mark a notable enhancement over the initial production levels and
524 highlight the importance of glycine and *L*-serine in shinorine biosynthesis, relying on amino acid
525 supplementation for large-scale production is not a feasible solution. Consequently, further
526 genetic alterations are imperative to improve *de novo* biosynthesis of glycine and *L*-serine. Our
527 CRISPRi studies have pinpointed genes potentially involved in glycine and *L*-serine metabolism.
528 However, the results indicated that none of the downregulated genes associated with glycine and
529 *L*-serine metabolism appeared to improve shinorine titer. This was rather expected, given that
530 many reactions in glycine and *L*-serine metabolism involve more than one gene (Fig. 4A). While
531 single-gene downregulation by CRISPRi was verified by shotgun proteomics, compensatory
532 mechanisms involving other enzymes likely mitigated the impact of individual gene knockdowns.
533 To overcome this challenge, future efforts must explore the synergistic effects of multiplexed
534 CRISPRi, facilitating simultaneous knockdowns of multiple genes. This strategic approach not

535 only promises a more profound impact on target pathways, but also presents an avenue for
 536 deciphering the dynamics of metabolic networks, ultimately optimizing them for improved
 537 shinorine production.
 538

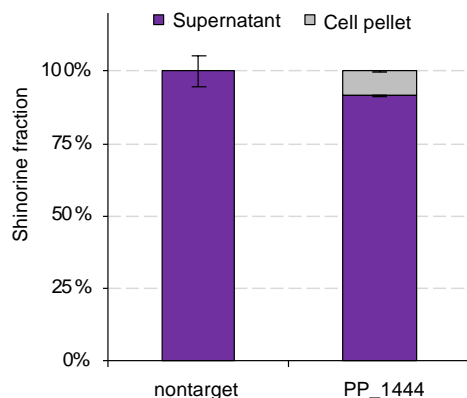


539
 540 Figure 6. Effects of glycine and L-serine supplementation on shinorine production. (A) Schematics of genetics
 541 constructs used in the study. *P. putida* KT2440, carrying the shinorine biosynthetic pathway plasmid (JBx_250497),
 542 was transformed with a CRISPRi plasmid containing either PP_1444 sgRNA (JBx_249619) or nontarget sgRNA
 543 (JBx_249575). (B,C) Comparison of shinorine production, glucose consumption, and growth profiles over a 114-hour
 544 period without glycine and L-serine supplementation. (D) Experimental conditions used in B, C, E, and F. (E,F)
 545 Comparison of shinorine production, glucose consumption, and growth profiles over a 114-hour period with glycine and
 546 L-serine supplementation. All strains were cultivated in 25 mL M9 medium containing 20 g/L glucose with a starting
 547 OD600 of 0.1. At 4 hr post inoculation, cultures were induced with 0.2% L-arabinose, with or without the addition of 10
 548 mM equimolar concentration of glycine and L-serine. At 18 hr, all cultures received an additional 20 g/L glucose. For
 549 samples in (D) and (F), an extra 20 g/L glucose was introduced to the cultures at the 42-hr time point. (Heberle et al.,
 550 2015) Error bars represent standard deviations from three biological replicates.
 551

552 Following the extraction of samples from the whole liquid cultures, we also extracted
553 shinorine from different fractions. The results unveiled that shinorine was found exclusively in the
554 supernatant in the control strain (nontarget sgRNA) whereas for the PP_1444 strain, 91% and 9%
555 shinorine was found in the supernatant and cell pellet, respectively (Fig. 7, Supplementary Fig.
556 S16). To our knowledge, a specific *P. putida* transporter for shinorine is currently not known.
557 However, our shotgun proteomics analysis revealed that the expression of several ABC efflux
558 systems, transporters, and outer membrane efflux proteins was altered in the PP_1444 strain
559 (Supplementary Table S4 and S5). These findings hint at the potential involvement of transporters
560 in facilitating the export or import of shinorine in *P. putida* KT2440. However, further in-depth
561 investigations are required to elucidate the precise mechanism and identify the specific
562 transporter responsible for these transport processes.

563 From a biotechnological downstream processing perspective, the exclusive secretion of
564 shinorine to the supernatant added significance to the use of *P. putida* KT2440 as a microbial
565 platform for shinorine production. When the shinorine accumulates in the liquid medium rather
566 than within the cells, it has several significant advantages for industrial biotechnology. Products
567 in the supernatant can be harvested more easily as there is no need for cell disruption which
568 simplifies the downstream processing and reduces costs (Ying Wang et al., 2019). It might also
569 require less rigorous purification steps, which can be advantageous from a cost perspective.
570 Additionally, if the product is secreted into the medium, the process could be adapted to a
571 continuous production system where the product is continuously harvested while the culture is
572 maintained. Accumulation of products within the cells can often lead to stress and eventual cell
573 death (Cray et al., 2015). Secretion avoids this issue, maintaining cell viability and potentially
574 increasing the overall yield of shinorine.

575



576
577 Fig. 7. Fraction of shinorine found in supernatant and cell pellet measured at 114 hr from samples in Fig. 6F. Error
578 bars represent standard deviations from three biological replicates.

579 **3. Materials and Methods**

580 **3.1 Strains, plasmids, media, and growth conditions**

581 *E. coli* XL 1-Blue strain (Thermo Fisher Scientific) was used to propagate all the plasmids
582 used in the study. The strain was routinely cultivated in lysogeny broth (LB) medium (LB Broth,
583 Sigma Aldrich), 37 °C, 180 rpm, and supplemented with appropriate antibiotic(s) (final
584 concentration: gentamicin 10 µg/mL, and kanamycin 50 µg/mL). Plasmids were constructed using
585 a modular plasmid assembly method, namely Biopart Assembly Standard Idempotent Cloning
586 (BASIC) (Storch et al., 2015) with modification.

587 Self replicating plasmids (RK2 and RSF1010-based plasmids) were transformed into
588 *Pseudomonas putida* KT2440 by electroporation. The electroporation procedure was modified
589 from (Choi et al., 2006). Briefly, one fresh colony of *P. putida* KT2440 was inoculated into 5 mL
590 of LB and incubated for overnight at 30 °C, 200 rpm. Overnight culture was centrifuged for 1 min
591 at 13,000 x *g*, washed three times with 1 mL 10% glycerol, and resuspended in 500 µL of 10%
592 glycerol at room temperature. Electroporation was performed by adding approximately 100 ng
593 DNA into 100 µL cell aliquot and shocked with Bio-Rad GenePulser II (USA) using 1 mm cuvette
594 (1.8k kV, 200 Ω). After electroporation, a volume of 1 mL LB media was added into the cuvette
595 and the cell mixtures were transferred into a fresh 1.5 mL microtube. For cell recovery, the cell
596 mixtures were allowed to grow at 30 °C, 200 rpm, for 1 h. After incubation, 20 µL of cell mixtures
597 was plated onto a selective agar plate containing appropriate antibiotic and incubated at 30 °C
598 overnight. Plasmids used in this study are listed in Supplementary Table S7.

599 *P. putida* KT2440 seed cultures were inoculated from single colonies and grown in 5 mL
600 LB medium at 30 °C, 180 rpm, overnight. Unless stated otherwise, 100 µL of the overnight cultures
601 were transferred into 5 mL of M9 minimal medium (Banerjee et al., 2024), and incubated at 30
602 °C, 180 rpm, overnight. This process was repeated one more time to allow complete adaptation
603 to M9 medium. For shinorine production, unless otherwise indicated, cell cultures were inoculated
604 at an OD₆₀₀ of 0.2 in 5 mL of M9 medium supplemented with 2% glucose and appropriate
605 antibiotics (kanamycin 50 mg/L, gentamicin 10 mg/L), and induced with 0.2% (w/v) *L*-arabinose
606 at 4 hr post-inoculation.

607

608 **3.2 Routine shinorine extraction and analysis**

609 For routine shinorine analysis from a whole liquid culture, 100 µL of liquid culture was
610 mixed with 250 µL of methanol and 125 µL of chloroform. The resulting mixture was vortexed for
611 5 min at 3,000 rpm. Next, 125 µL of ultrapure water and 100 µL of chloroform were added and
612 the samples were re-vortexed for 5 min at 3000 rpm followed by centrifugation for 1 min at 13,000

613 x g. Shinorine was then sampled from the top aqueous layer and measured using a NanoDrop™
614 2000/2000c Spectrophotometers at 334 nm. To determine the concentration of shinorine in the
615 sample, serially diluted purified shinorine standards were prepared and the concentration was
616 determined using the Beer-lambert law with ϵ = extinction coefficient of shinorine
617 ($\epsilon = 44,700 \text{ M}^{-1} \text{ cm}^{-1}$). (Llewellyn et al., 2020; Wada et al., 2015).

618 For the analysis of extracellular shinorine, 100 μL of liquid culture was centrifuged for 5
619 min at 13,000 x g, and shinorine was measured from the supernatant without extraction. For the
620 analysis of intracellular shinorine, 100 μL of liquid culture was centrifuged for 5 min at 13,000 x g.
621 The supernatant was removed, and the cell pellet was washed three times with 500 μL of ultrapure
622 water. Finally, the cell pellet was resuspended in 100 μL of ultrapure water and mixed with 250
623 μL of methanol and 125 μL of chloroform, following the extraction method described above for the
624 whole liquid culture.

625

626 **3.3 Construction of CRISPRi plasmids**

627 For CRISPRi-mediated gene downregulation, single guide RNAs (sgRNAs) with 22
628 nucleotide sequences were designed using the web tool CRISPOR (Concordet and Haeussler,
629 2018) to target the non-template strand with NGG protospacer adjacent motif (PAM) sequence.
630 A pair of complementary DNA oligos was ordered from Integrated DNA Technologies, hybridized
631 at 95 °C for 10 min, and cooled down to room temperature in a heating block. Hybridized oligo
632 was digested with *BsaI* (New England Biolabs) and ligated to *PaqCI*-digested pLY993 plasmid
633 (JBx_249165). The resulting plasmid was digested with *BsaI* and cloned into pLY989 plasmid
634 (JBx_249567). Hybridized oligos used for CRISPRi-mediated gene downregulation are listed in
635 Supplementary Table S8.

636

637 **3.4 Fluorescence measurement**

638 Fluorescence measurement was done using a flow cytometer, 2 mL of LB media was
639 inoculated with overnight culture (0.1% v/v) and supplemented with appropriate antibiotics. After
640 24 hr of incubation, 1-3 μL of samples was added to 150 μL 1X phosphate buffered saline. Single-
641 cell RFP and GFP fluorescence from at least 30,000 cells was immediately recorded using a BD
642 C6 Accuri flow cytometer (BD Bioscience). GFP and RFP fluorescence was measured using FL1
643 and FL4 detector, respectively. Protein fluorescent level was determined by taking the average of
644 the fluorescence distribution.

645

646 **3.5 Shinorine standard preparation**

647 Shinorine-producing strain was cultivated in 250 mL M9 medium in a 1-L flask with a
648 starting OD₆₀₀ 0.2. At 48 hr post inoculation, sample was centrifuged at 4 °C, 4,500 x g for 30 min.
649 To concentrate and desalt shinorine from the culture supernatant, the supernatant was loaded
650 onto a HyperCarb 2G SPE column (Thermo Scientific), washed with 10 mL of 5% acetonitrile,
651 and eluted with 10 mL of 80% acetonitrile. The eluent was evaporated to dryness on a LabConco
652 SpeedVac. The dried SPE elution was then reconstituted in MilliQ water and semi-purified using
653 an Agilent 1260 HPLC system equipped with a Machery-Nagel Nucleosil 100-10 SB strong anion
654 exchange column (250 mm x 4.6 mm, 10 µm particle size) operating at a flow rate of 1 mL/min
655 using an isocratic mobile phase composed of 25 mM LC-MS grade ammonium bicarbonate
656 (Fisher Scientific). Fractions were manually collected by monitoring the absorbance of the
657 shinorine chromophore ($\lambda = 334$ nm). The observed retention time for shinorine was
658 approximately 12.4 minutes. Collected fractions were then evaporated to dryness on a LabConco
659 SpeedVac.

660 Dried fractions from anion exchange semi-purification were reconstituted in water and
661 injected onto an Agilent 1260 HPLC system equipped with a Thermo HyperCarb column (150 mm
662 x 4.6 mm, 5 µm particle size) operating at 1.5 mL/min using the following gradient (A = 0.3%
663 ammonium formate pH 9.0, B = acetonitrile): 0 min 2% B, 20 min 15% B, 26 min 50% B, 27-33
664 min 90% B, 35-40 min 2% B. Fractions were manually collected by monitoring the absorbance of
665 the shinorine chromophore ($\lambda = 334$ nm). The observed retention time for shinorine was
666 approximately 9.2 minutes. Fractions containing shinorine were then flash frozen in liquid nitrogen
667 and placed on a LabConco lyophilizer. The dried fractions were reconstituted in water, frozen,
668 and lyophilized three times to volatilize residual ammonium formate. The resulting dried solid of
669 purified shinorine was then used for characterization by NMR spectroscopy.

670

671 **3.6 NMR spectroscopy of purified shinorine**

672 Approximately 4.6 mg of purified shinorine was dissolved in 400 µL methanol-*d*₄ with
673 0.03% trimethylsilane (>99.8% atom % D; Sigma-Aldrich). NMR spectra were obtained on a
674 Bruker Avance NEO 500 MHz equipped with a 5 mm ¹H/BB iProbe. Samples were held at 298 K
675 during acquisition. Standard Bruker pulse sequences were used for each of the following
676 experiments: ¹H, ¹³C, ¹H-¹H COSY, ¹H-¹H NOESY (750 ms mixing time), ¹H-¹³C HSQC, and ¹H-
677 ¹³C HMBC. Spectra were recorded using the Bruker TopSpin 4.0.6 software and analyzed using
678 MestReNova 14.3.2. Chemical shifts (δ , ppm) were referenced internally to trimethylsilane.

679

680 **3.7 Proteomics analysis**

681 Protein was extracted from cell pellets and tryptic peptides were prepared by following
682 established proteomic sample preparation protocol (Chen et al., 2023) Briefly, cell pellets were
683 resuspended in Qiagen P2 Lysis Buffer (Qiagen, Germany) to promote cell lysis. Proteins were
684 precipitated with addition of 1 mM NaCl and 4 x vol acetone, followed by two additional washes
685 with 80% acetone in water. The recovered protein pellet was homogenized by pipetting mixing
686 with 100 mM ammonium bicarbonate in 20% methanol. Protein concentration was determined by
687 the DC protein assay (BioRad, USA). Protein reduction was accomplished using 5 mM tris 2-
688 (carboxyethyl)phosphine (TCEP) for 30 min at room temperature, and alkylation was performed
689 with 10 mM iodoacetamide (IAM; final concentration) for 30 min at room temperature in the dark.
690 Overnight digestion with trypsin was accomplished with a 1:50 trypsin:total protein ratio. The
691 resulting peptide samples were analyzed on an Agilent 1290 UHPLC system coupled to a Thermo
692 Scientific Orbitrap Exploris 480 mass spectrometer for discovery proteomics (Chen et al., 2020).
693 Briefly, peptide samples were loaded onto an Ascentis® ES-C18 Column (Sigma–Aldrich, USA)
694 and were eluted from the column by using a 10 minute gradient from 98% solvent A (0.1 % FA in
695 H₂O) and 2% solvent B (0.1% FA in ACN) to 65% solvent A and 35% solvent B. Eluting peptides
696 were introduced to the mass spectrometer operating in positive-ion mode and were measured in
697 data-independent acquisition (DIA) mode with a duty cycle of 3 survey scans from m/z 380 to m/z
698 985 and 45 MS₂ scans with precursor isolation width of 13.5 m/z to cover the mass range. DIA
699 raw data files were analyzed by an integrated software suite DIA-NN (Demichev et al., 2020). The
700 database used in the DIA-NN search (library-free mode) was *P. putida* KT2440 latest Uniprot
701 proteome FASTA sequences plus the protein sequences of the heterologous proteins and
702 common proteomic contaminants. DIA-NN determines mass tolerances automatically based on
703 first pass analysis of the samples with automated determination of optimal mass accuracies. The
704 retention time extraction window was determined individually for all MS runs analyzed via the
705 automated optimization procedure implemented in DIA-NN. Protein inference was enabled, and
706 the quantification strategy was set to Robust LC = High Accuracy. Output main DIA-NN reports
707 were filtered with a global FDR = 0.01 on both the precursor level and protein group level. The
708 Top3 method, which is the average MS signal response of the three most intense tryptic peptides
709 of each identified protein, was used to plot the quantity of the targeted proteins in the samples
710 (Ahrné et al., 2013; Silva et al., 2006). The generated mass spectrometry proteomics data have
711 been deposited to the ProteomeXchange Consortium via the PRIDE partner repository with the
712 dataset identifier PXD050908 (Perez-Riverol et al., 2022).

713

714 **3.8 Metabolomics analysis**

715 The LC-MS/MS analysis was conducted on a Kinetex XB-C18 column (100-mm length,
716 3.0-mm internal diameter, and 2.6- μ m particle size; Phenomenex, Torrance, CA USA) using a
717 1260 Infinity HPLC system (Agilent Technologies, Santa Clara, CA, USA). A sample injection
718 volume of 2 μ L was used throughout. The sample tray and column compartment were set to 6
719 and 20 °C, respectively. The mobile phase was composed of 10 mM ammonium formate and 0.2
720 % formic acid (Sigma-Aldrich, St. Louis, MO, USA) in water (solvent A) and 10 mM ammonium
721 formate and 0.2 % formic acid in 90% acetonitrile and 9.8% water (solvent B). Shinorine was
722 separated via gradient elution under the following conditions: linearly decreased from 90 %B to
723 70 %B in 4 min, held at 70 %B for 1.5 min, linearly decreased from 70 %B to 40 % B in 0.5 min,
724 held at 40 %B for 2.5 min, linearly increased form 40 %B to 90 %B in 0.5 min, held at 90 %B for
725 2 min. The flow rate was held at 0.6 mL/min for 6.5 min, linearly increased from 0.6 mL/min to 1
726 mL/min in 0.5 min, held at 1 mL/min for 4 min. The total LC run time was 11 min. The HPLC
727 system was coupled to an Agilent Technologies 6520 quadrupole time-of-flight mass
728 spectrometer (for LC-QTOF-MS). The QTOF-MS was tuned with Agilent Technologies ESI-L Low
729 concentration tuning mix in the range of 50-1700 m/z. Drying and nebulizing gases were set to 12
730 L/min and 25 lb/in², respectively, and a drying-gas temperature of 350 °C was used throughout.
731 Electrospray ionization was conducted in the positive ion mode (for [M + H]⁺ ions) and a capillary
732 voltage of 3500 V was utilized. The fragmentor, skimmer, and OCT 1 RF Vpp voltages were set
733 to 100 V, 50 V, and 250 V, respectively. For targeted MS/MS, a precursor ion of 333.12942 m/z
734 was selected for collision induced dissociation at a collision energy of 30 eV with a narrow isolation
735 width of 1.3 m/z. The acquisition rate was 1 spectra/s. The data acquisition range was from 40-
736 1100 m/z. Data acquisition (Workstation B.08.00) and processing (Qualitative Analysis B.06.00)
737 were conducted via Agilent Technologies MassHunter software.

738

739 **3.9 Carbon flux distribution prediction by genome-scale metabolic models**

740 Genome-scale metabolic models were used to predict the flux sum (Chung and Lee, 2009)
741 around 6-phosphogluconate. Metabolic flux distribution in a glucose minimal medium was first
742 predicted by parsimonious flux balance analysis (Lewis et al., 2010), and the sum of all incoming
743 or outgoing fluxes around 6-phosphogluconate was calculated and normalized by the glucose
744 uptake rate for each model.

745

746 **4. Conclusion**

747 Growing interest in sourcing a sustainable and environmentally friendly sunscreen has
748 motivated scientists to produce shinorine, a naturally occurring compound with UV-absorbing

749 properties, in microbes. Our study provides a comprehensive approach for engineering
750 *Pseudomonas putida* KT2440 as an efficient chassis for shinorine production. Comprehensive
751 review of metabolic flux distribution from different microbes pinpoint *P. putida* KT2440 as a
752 potential host for shinorine production. By leveraging synthetic biology approaches and metabolic
753 engineering strategies, we have significantly increased shinorine yield and productivity CRISPRi-
754 mediated gene downregulation, particularly targeting the PP_1444 gene, significantly improved
755 shinorine production compared to the first-engineered strain. Proteomics analysis shows
756 downregulation of PP_1444 has far-reaching effects on the expression of multiple genes in *P.*
757 *putida* KT2440. Refinement of genetic design, promoter usage, and ribosome binding sites also
758 contributed to the titer improvement. Feeding studies indicate that the supply of two critical amino
759 acids, *L*-serine and glycine, might be the limiting factor in shinorine biosynthesis. The final titer,
760 productivity, and yield of 900 mg/L, 10 mg/L/h, and 22.5 mg/g glucose (without glycine and *L*-
761 serine supplementation) and 1,601 mg/L, 14 mg/L/h, and 26 – 28.35 mg/g glucose (with glycine
762 and *L*-serine supplementation), respectively, represent a substantial improvement over the initial
763 production levels and surpass achievements of earlier studies. Additionally, the exclusive
764 secretion of shinorine into the culture medium offers advantages for downstream processing in
765 industrial applications. These findings underscore the potential of *P. putida* KT2440 as a microbial
766 platform to produce valuable natural compounds. Through continued optimization and scale-up
767 efforts, our work paves the way for the commercialization of shinorine as a bio-based alternative
768 in the sunscreen industry.

769

770 **5. Acknowledgement**

771 We thank Drs. Hasan Celik, Raynald Giovine, and Pines Magnetic Resonance Center's
772 Core NMR Facility (PMRC Core) for spectroscopic assistance. This material is based upon work
773 supported by the Joint BioEnergy Institute (<http://www.jbei.org>), U.S. Department of Energy,
774 Office of Science, Biological and Environmental Research Program under Award Number DE-
775 AC02-05CH11231 with Lawrence Berkeley National Laboratory. The instruments used in this
776 work were supported by the PMRC Core. Pacific Northwest National Laboratory portion is
777 operated for the U.S. Department of Energy by Battelle under Contract DE-AC05-76RL01830.
778 The United States Government retains a non-exclusive, paid-up, irrevocable, worldwide license
779 to publish or reproduce the published form of this manuscript, or permit others to do so, for United
780 States Government purposes. The views and opinions expressed by the authors do not
781 necessarily reflect those of the United States Government or any of its agencies. The United
782 States Government and its employees make no warranty, expressed or implied, regarding the

783 accuracy, completeness, or usefulness of any information, apparatus, product, or process
784 disclosed, nor do they represent that the use of such information would not infringe privately
785 owned rights.

786

787 **6. Author Contributions**

788 Conceptualization and design of the project: Yunus, Lee. Acquisition of data: Yunus,
789 Hudson, Chen, Gin, Baidoo. Analysis and interpretation of data: Yunus, Hudson, Chen, Kim,
790 Baidoo, Petzold, Lee. Drafting of manuscript: Yunus, Hudson, Chen, Kim, Baidoo, Petzold, Lee.
791 Critical revision: Yunus, Hudson, Kim, Baidoo, Petzold, Adams, Simmons, Mukhopadhyay,
792 Keasling, Lee. Funding acquisition: Adams, Simmons, Mukhopadhyay, Keasling, Lee. All authors
793 contributed to and provided feedback on the manuscript. All authors read and approved the final
794 manuscript.

795

796 **7. Competing Interests**

797 The authors declare no competing interests.

798

799 **8. Supporting Information**

800 Supplementary Figures and Supplementary Tables are available in a separate pdf file
801 ("Supporting Information.pdf").

802

803 **References**

804

805 Ahrné, E., Molzahn, L., Glatter, T., Schmidt, A., 2013. Critical assessment of proteome-wide
806 label-free absolute abundance estimation strategies. *Proteomics* 13, 2567–2578.

807 <https://doi.org/https://doi.org/10.1002/pmic.201300135>

808 Aidelberg, G., Towbin, B.D., Rothschild, D., Dekel, E., Bren, A., Alon, U., 2014. Hierarchy of
809 non-glucose sugars in *Escherichia coli*. *BMC Syst Biol* 8, 133.

810 <https://doi.org/10.1186/s12918-014-0133-z>

811 Anderson, Jc., Dueber, J.E., Leguia, M., Wu, G.C., Goler, J.A., Arkin, A.P., Keasling, J.D., 2010.
812 BglBricks: A flexible standard for biological part assembly. *J Biol Eng* 4, 1.

813 <https://doi.org/10.1186/1754-1611-4-1>

814 Antoine, R., Locht, C., 1992. Isolation and molecular characterization of a novel broad-host-

815 range plasmid from *Bordetella bronchiseptica* with sequence similarities to plasmids from

816 Gram-positive organisms. *Mol Microbiol* 6, 1785–1799.
817 <https://doi.org/https://doi.org/10.1111/j.1365-2958.1992.tb01351.x>

818 Aparicio, T., de Lorenzo, V., Martínez-García, E., 2019. Improved Thermotolerance of Genome-
819 Reduced *Pseudomonas putida* EM42 Enables Effective Functioning of the PL/cl857
820 System. *Biotechnol J* 14, 1800483. <https://doi.org/https://doi.org/10.1002/biot.201800483>

821 Aparicio, T., Nyerges, A., Martínez-García, E., de Lorenzo, V., 2020. High-Efficiency Multi-site
822 Genomic Editing of *Pseudomonas putida* through Thermoinducible ssDNA
823 Recombineering. *iScience* 23, 100946.
824 <https://doi.org/https://doi.org/10.1016/j.isci.2020.100946>

825 Bagdasarian, M.M., Amann, E., Lurz, R., Rückert, B., Bagdasarian, M., 1983. Activity of the
826 hybrid *trp-lac* (*tac*) promoter of *Escherichia coli* in *Pseudomonas putida*. Construction of
827 broad-host-range, controlled-expression vectors. *Gene* 26, 273–282.
828 [https://doi.org/https://doi.org/10.1016/0378-1119\(83\)90197-X](https://doi.org/https://doi.org/10.1016/0378-1119(83)90197-X)

829 Balskus, E.P., Walsh, C.T., 2010. The Genetic and Molecular Basis for Sunscreen Biosynthesis
830 in Cyanobacteria. *Science* (1979) 329, 1653–1656.
831 <https://doi.org/10.1126/science.1193637>

832 Banerjee, D., Eng, T., Lau, A.K., Sasaki, Y., Wang, B., Chen, Y., Prah, J.-P., Singan, V.R.,
833 Herbert, R.A., Liu, Y., Tanjore, D., Petzold, C.J., Keasling, J.D., Mukhopadhyay, A., 2020.
834 Genome-scale metabolic rewiring improves titers rates and yields of the non-native product
835 indigoidine at scale. *Nat Commun* 11, 5385. <https://doi.org/10.1038/s41467-020-19171-4>

836 Banerjee, D., Yunus, I.S., Wang, X., Kim, Jinho, Srinivasan, A., Menchavez, R., Chen, Y., Gin,
837 J.W., Petzold, C.J., Martin, H.G., Magnuson, J.K., Adams, P.D., Simmons, B.A.,
838 Mukhopadhyay, A., Kim, Joonhoon, Lee, T.S., 2024. Genome-scale and pathway
839 engineering for the sustainable aviation fuel precursor isoprenol production in
840 *Pseudomonas putida*. *Metab Eng* 82, 157–170.
841 <https://doi.org/https://doi.org/10.1016/j.ymben.2024.02.004>

842 Becker, K., Hartmann, A., Ganzera, M., Fuchs, D., Gostner, J.M., 2016. Immunomodulatory
843 effects of the mycosporine-like amino acids shinorine and porphyra-334. *Mar. Drugs* 14,
844 119.

845 Bentley, G.J., Narayanan, N., Jha, R.K., Salvachúa, D., Elmore, J.R., Peabody, G.L., Black,
846 B.A., Ramirez, K., De Capite, A., Michener, W.E., Werner, A.Z., Klingeman, D.M.,
847 Schindel, H.S., Nelson, R., Foust, L., Guss, A.M., Dale, T., Johnson, C.W., Beckham, G.T.,
848 2020. Engineering glucose metabolism for enhanced muconic acid production in

849 *Pseudomonas putida* KT2440. *Metab Eng* 59, 64–75.
850 <https://doi.org/https://doi.org/10.1016/j.ymben.2020.01.001>

851 Bommareddy, R.R., Sabra, W., Maheshwari, G., Zeng, A.-P., 2015. Metabolic network analysis
852 and experimental study of lipid production in *Rhodospiridium toruloides* grown on single
853 and mixed substrates. *Microb Cell Fact* 14, 36. <https://doi.org/10.1186/s12934-015-0217-5>

854 Brink, D.P., Mierke, F., Norbeck, J., Siewers, V., Andlid, T., 2023. Expanding the genetic toolbox
855 of *Rhodotorula toruloides* by identification and validation of six novel promoters induced or
856 repressed under nitrogen starvation. *Microb Cell Fact* 22, 160.
857 <https://doi.org/10.1186/s12934-023-02175-2>

858 Calero, P., Jensen, S.I., Nielsen, A.T., 2016. Broad-Host-Range ProUSER Vectors Enable Fast
859 Characterization of Inducible Promoters and Optimization of p-Coumaric Acid Production in
860 *Pseudomonas putida* KT2440. *ACS Synth Biol* 5, 741–753.
861 <https://doi.org/10.1021/acssynbio.6b00081>

862 Chen, Y., Gin, J., Petzold, C., 2020. Discovery proteomic (DDA) LC-MS/MS data acquisition
863 and analysis. *protocols.io*. <https://dx.doi.org/10.17504/protocols.io.bgbqjismw>.

864 Chen, Y., Gin, J.W., Wang, Y., de Raad, M., Tan, S., Hillson, N.J., Northen, T.R., Adams, P.D.,
865 Petzold, C.J., 2023. Alkaline-SDS cell lysis of microbes with acetone protein precipitation
866 for proteomic sample preparation in 96-well plate format. *PLoS One* 18, e0288102-.

867 Choi, K.-H., Kumar, A., Schweizer, H.P., 2006. A 10-min method for preparation of highly
868 electrocompetent *Pseudomonas aeruginosa* cells: Application for DNA fragment transfer
869 between chromosomes and plasmid transformation. *J. Microbiol. Methods* 64, 391.

870 Choi, Y.-H., Yang, D.J., Kulkarni, A., Moh, S.H., Kim, K.W., 2015. Mycosporine-Like Amino
871 Acids Promote Wound Healing through Focal Adhesion Kinase (FAK) and Mitogen-
872 Activated Protein Kinases (MAP Kinases) Signaling Pathway in Keratinocytes. *Mar Drugs*
873 13, 7055–7066. <https://doi.org/10.3390/md13127056>

874 Chung, B.K.S., Lee, D.-Y., 2009. Flux-sum analysis: a metabolite-centric approach for
875 understanding the metabolic network. *BMC Syst Biol* 3, 117. <https://doi.org/10.1186/1752-0509-3-117>

877 Concordet, J.-P., Haeussler, M., 2018. CRISPOR: intuitive guide selection for CRISPR/Cas9
878 genome editing experiments and screens. *Nucleic Acids Res* 46, W242–W245.
879 <https://doi.org/10.1093/nar/gky354>

880 Cook, T.B., Rand, J.M., Nurani, W., Courtney, D.K., Liu, S.A., Pflieger, B.F., 2018. Genetic tools
881 for reliable gene expression and recombineering in *Pseudomonas putida*. *J Ind Microbiol*
882 *Biotechnol* 45, 517–527. <https://doi.org/10.1007/s10295-017-2001-5>

883 Cray, J.A., Stevenson, A., Ball, P., Bankar, S.B., Eleutherio, E.C.A., Ezeji, T.C., Singhal, R.S.,
884 Thevelein, J.M., Timson, D.J., Hallsworth, J.E., 2015. Chaotropicity: a key factor in product
885 tolerance of biofuel-producing microorganisms. *Curr Opin Biotechnol* 33, 228–259.
886 <https://doi.org/https://doi.org/10.1016/j.copbio.2015.02.010>

887 Damalas, S.G., Batiannis, C., Martin-Pascual, M., de Lorenzo, V., Martins dos Santos, V.A.P.,
888 2020. SEVA 3.1: enabling interoperability of DNA assembly among the SEVA, BioBricks
889 and Type IIS restriction enzyme standards. *Microb Biotechnol* 13, 1793–1806.
890 <https://doi.org/https://doi.org/10.1111/1751-7915.13609>

891 De Bernardez, E.R., Dhurjati, P.S., 1987. Effect of a broad-host range plasmid on growth
892 dynamics of *Escherichia coli* and *Pseudomonas putida*. *Biotechnol Bioeng* 29, 558–565.
893 <https://doi.org/https://doi.org/10.1002/bit.260290504>

894 De Graaf, A.A., Striegel, K., Wittig, R.M., Laufer, B., Schmitz, G., Wiechert, W., Sprenger, G.A.,
895 Sahm, H., 1999. Metabolic state of *Zymomonas mobilis* in glucose-, fructose-, and xylose-
896 fed continuous cultures as analysed by ¹³C- and ³¹P-NMR spectroscopy. *Arch Microbiol*
897 171, 371–385. <https://doi.org/10.1007/s002030050724>

898 Demichev, V., Messner, C.B., Vernardis, S.I., Lilley, K.S., Ralser, M., 2020. DIA-NN: neural
899 networks and interference correction enable deep proteome coverage in high throughput.
900 *Nat Methods* 17, 41–44. <https://doi.org/10.1038/s41592-019-0638-x>

901 Dvořák, P., de Lorenzo, V., 2018. Refactoring the upper sugar metabolism of *Pseudomonas*
902 *putida* for co-utilization of cellobiose, xylose, and glucose. *Metab Eng* 48, 94–108.
903 <https://doi.org/https://doi.org/10.1016/j.ymben.2018.05.019>

904 Elmore, J.R., Furches, A., Wolff, G.N., Gorday, K., Guss, A.M., 2017. Development of a high
905 efficiency integration system and promoter library for rapid modification of *Pseudomonas*
906 *putida* KT2440. *Metab Eng Commun* 5, 1–8.
907 <https://doi.org/https://doi.org/10.1016/j.meteno.2017.04.001>

908 Fang, L., Fan, J., Luo, S., Chen, Y., Wang, C., Cao, Y., Song, H., 2021. Genome-scale target
909 identification in *Escherichia coli* for high-titer production of free fatty acids. *Nat Commun*
910 12, 4976. <https://doi.org/10.1038/s41467-021-25243-w>

911 Farinha, M.A., Kropinski, A.M., 1990. Construction of broad-host-range plasmid vectors for easy
912 visible selection and analysis of promoters. *J Bacteriol* 172, 3496–3499.
913 <https://doi.org/10.1128/jb.172.6.3496-3499.1990>

914 Hartmann, A.; Gostner, J.; Fuchs, J.; Chaita, E.; Aligiannis, N.; Skaltsounis, L.; Ganzera, M.,
915 2015. Inhibition of Collagenase by Mycosporine-like Amino Acids from Marine Sources.
916 *Planta Med* 81, 813–820. <https://doi.org/10.1055/s-0035-1546105>

917 Hüsken, L., Beeftink, R., de Bont, J., Wery, J., 2001. High-rate 3-methylcatechol production in
918 *Pseudomonas putida* strains by means of a novel expression system. *Appl Microbiol*
919 *Biotechnol* 55, 571–577. <https://doi.org/10.1007/s002530000566>

920 Itoh, Y., Haas, D., 1985. Cloning vectors derived from the *Pseudomonas* plasmid pVS1. *Gene*
921 36, 27–36. [https://doi.org/https://doi.org/10.1016/0378-1119\(85\)90066-6](https://doi.org/https://doi.org/10.1016/0378-1119(85)90066-6)

922 Jacobson, T.B., Adamczyk, P.A., Stevenson, D.M., Regner, M., Ralph, J., Reed, J.L., Amador-
923 Noguez, D., 2019. 2H and 13C metabolic flux analysis elucidates in vivo thermodynamics
924 of the ED pathway in *Zymomonas mobilis*. *Metab Eng* 54, 301–316.
925 <https://doi.org/https://doi.org/10.1016/j.ymben.2019.05.006>

926 Jeschek, M., Gerngross, D., Panke, S., 2017. Combinatorial pathway optimization for
927 streamlined metabolic engineering. *Curr Opin Biotechnol* 47, 142–151.
928 <https://doi.org/https://doi.org/10.1016/j.copbio.2017.06.014>

929 Jin, C., Kim, S., Moon, S., Jin, H., Hahn, J.-S., 2021. Efficient production of shinorine, a natural
930 sunscreen material, from glucose and xylose by deleting HXK2 encoding hexokinase in
931 *Saccharomyces cerevisiae*. *FEMS Yeast Res.* 21, foab053.

932 Jin, H., Kim, S., Lee, D., Ledesma-Amaro, R., Hahn, J.-S., 2023. Efficient production of
933 mycosporine-like amino acids, natural sunscreens, in *Yarrowia lipolytica*. *Biotechnology for*
934 *Biofuels and Bioproducts* 16, 162. <https://doi.org/10.1186/s13068-023-02415-y>

935 Johnson, J. V, Dick, J.T.A., Pincheira-Donoso, D., 2022. Marine protected areas do not buffer
936 corals from bleaching under global warming. *BMC Ecol Evol* 22, 58.
937 <https://doi.org/10.1186/s12862-022-02011-y>

938 Jones, J.A., Toparlak, Ö.D., Koffas, M.A.G., 2015. Metabolic pathway balancing and its role in
939 the production of biofuels and chemicals. *Curr Opin Biotechnol* 33, 52–59.
940 <https://doi.org/https://doi.org/10.1016/j.copbio.2014.11.013>

941 Kaczmarzyk, D., Cengic, I., Yao, L., Hudson, E.P., 2018. Diversion of the long-chain acyl-ACP
942 pool in *Synechocystis* to fatty alcohols through CRISPRi repression of the essential
943 phosphate acyltransferase PlsX. *Metab Eng* 45, 59–66.
944 <https://doi.org/https://doi.org/10.1016/j.ymben.2017.11.014>

945 Kim, S., Park, B.G., Jin, H., Lee, D., Teoh, J.Y., Kim, Y.J., Lee, S., Kim, S.-J., Moh, S.H., Yoo,
946 D., Choi, W., Hahn, J.-S., 2023. Efficient production of natural sunscreens shinorine,
947 porphyra-334, and mycosporine-2-glycine in *Saccharomyces cerevisiae*. *Metab Eng* 78,
948 137–147. <https://doi.org/https://doi.org/10.1016/j.ymben.2023.05.009>

949 Kim, S.-R., Cha, M., Kim, T., Song, S., Kang, H.J., Jung, Y., Cho, J.-Y., Moh, S.H., Kim, S.-J.,
950 2022. Sustainable Production of Shinorine from Lignocellulosic Biomass by Metabolically

951 Engineered *Saccharomyces cerevisiae*. *J Agric Food Chem* 70, 15848–15858.
952 <https://doi.org/10.1021/acs.jafc.2c07218>

953 Kohlstedt, M., Wittmann, C., 2019. GC-MS-based ¹³C metabolic flux analysis resolves the
954 parallel and cyclic glucose metabolism of *Pseudomonas putida* KT2440 and *Pseudomonas*
955 *aeruginosa* PAO1. *Metab Eng* 54, 35–53.
956 <https://doi.org/https://doi.org/10.1016/j.ymben.2019.01.008>

957 Kukurugya, M.A., Mendonca, C.M., Solhtalab, M., Wilkes, R.A., Thannhauser, T.W., Aristilde,
958 L., 2019. Multi-omics analysis unravels a segregated metabolic flux network that tunes co-
959 utilization of sugar and aromatic carbons in *Pseudomonas putida*. *Journal of Biological*
960 *Chemistry* 294, 8464–8479. <https://doi.org/https://doi.org/10.1074/jbc.RA119.007885>

961 Lewis, N.E., Hixson, K.K., Conrad, T.M., Lerman, J.A., Charusanti, P., Polpitiya, A.D., Adkins,
962 J.N., Schramm, G., Purvine, S.O., Lopez-Ferrer, D., Weitz, K.K., Eils, R., König, R., Smith,
963 R.D., Palsson, B.Ø., 2010. Omic data from evolved *E. coli* are consistent with computed
964 optimal growth from genome‐scale models. *Mol Syst Biol* 6, 390.
965 <https://doi.org/https://doi.org/10.1038/msb.2010.47>

966 Liu, D., Geiselman, G.M., Coradetti, S., Cheng, Y.-F., Kirby, J., Prahl, J.-P., Jacobson, O.,
967 Sundstrom, E.R., Tanjore, D., Skerker, J.M., Gladden, J., 2020. Exploiting nonionic
968 surfactants to enhance fatty alcohol production in *Rhodospiridium toruloides*. *Biotechnol*
969 *Bioeng* 117, 1418–1425. <https://doi.org/https://doi.org/10.1002/bit.27285>

970 Liu, D., Hwang, H.J., Otoupal, P.B., Geiselman, G.M., Kim, Joonhoon, Pomraning, K.R., Kim,
971 Y.-M., Munoz, N., Nicora, C.D., Gao, Y., Burnum-Johnson, K.E., Jacobson, O., Coradetti,
972 S., Kim, Jinho, Deng, S., Dai, Z., Prahl, J.-P., Tanjore, D., Lee, T.S., Magnuson, J.K.,
973 Gladden, J.M., 2023. Engineering *Rhodospiridium toruloides* for production of 3-
974 hydroxypropionic acid from lignocellulosic hydrolysate. *Metab Eng* 78, 72–83.
975 <https://doi.org/https://doi.org/10.1016/j.ymben.2023.05.001>

976 Liu, T., Mazmouz, R., Pearson, L.A., Neilan, B.A., 2019. Mutagenesis of the Microcystin
977 Tailoring and Transport Proteins in a Heterologous Cyanotoxin Expression System. *ACS*
978 *Synth Biol* 8, 1187–1194. <https://doi.org/10.1021/acssynbio.9b00068>

979 Llewellyn, C.A., Greig, C., Silkina, A., Kultschar, B., Hitchings, M.D., Farnham, G., 2020.
980 Mycosporine-like amino acid and aromatic amino acid transcriptome response to UV and
981 far-red light in the cyanobacterium *Chlorogloeopsis fritschii* PCC 6912. *Sci Rep* 10, 20638.
982 <https://doi.org/10.1038/s41598-020-77402-6>

983 Miyamoto, K.T., Mamoru, K., Haruo, I., 2014. Discovery of Gene Cluster for Mycosporine-Like
984 Amino Acid Biosynthesis from Actinomycetales Microorganisms and Production of a Novel

985 Mycosporine-Like Amino Acid by Heterologous Expression. *Appl Environ Microbiol* 80,
986 5028–5036. <https://doi.org/10.1128/AEM.00727-14>

987 Nikel, P.I., Chavarría, M., Fuhrer, T., Sauer, U., de Lorenzo, V., 2015. *Pseudomonas*
988 *putida* KT2440 Strain Metabolizes Glucose through a Cycle Formed by Enzymes of
989 the Entner-Doudoroff, Embden-Meyerhof-Parnas, and Pentose Phosphate Pathways *.
990 *Journal of Biological Chemistry* 290, 25920–25932.
991 <https://doi.org/10.1074/jbc.M115.687749>

992 Nikel, P.I., de Lorenzo, V., 2018. *Pseudomonas putida* as a functional chassis for industrial
993 biocatalysis: From native biochemistry to trans-metabolism. *Metab Eng* 50, 142–155.
994 <https://doi.org/https://doi.org/10.1016/j.ymben.2018.05.005>

995 Niu, W., Willett, H., Mueller, J., He, X., Kramer, L., Ma, B., Guo, J., 2020. Direct biosynthesis of
996 adipic acid from lignin-derived aromatics using engineered *Pseudomonas putida* KT2440.
997 *Metab Eng* 59, 151–161. <https://doi.org/https://doi.org/10.1016/j.ymben.2020.02.006>

998 Noel Jr., R.J., Reznikoff, W.S., 2000. Structural Studies of *lac*UV5-RNA Polymerase
999 Interactions *in Vitro*: ETHYLATION INTERFERENCE AND MISSING
1000 NUCLEOSIDE ANALYSIS *. *Journal of Biological Chemistry* 275, 7708–7712.
1001 <https://doi.org/10.1074/jbc.275.11.7708>

1002 Oliver, E.C.J., Donat, M.G., Burrows, M.T., Moore, P.J., Smale, D.A., Alexander, L. V,
1003 Benthuisen, J.A., Feng, M., Sen Gupta, A., Hobday, A.J., Holbrook, N.J., Perkins-
1004 Kirkpatrick, S.E., Scannell, H.A., Straub, S.C., Wernberg, T., 2018. Longer and more
1005 frequent marine heatwaves over the past century. *Nat Commun* 9, 1324.
1006 <https://doi.org/10.1038/s41467-018-03732-9>

1007 Orfanoudaki, M., Hartmann, A., Alilou, M., Gelbrich, T., Planchenault, P., Derbré, S.,
1008 Schinkovitz, A., Richomme, P., Hensel, A., Ganzera, M., 2020. Absolute Configuration of
1009 Mycosporine-Like Amino Acids, Their Wound Healing Properties and *In Vitro* Anti-Aging
1010 Effects. *Mar Drugs* 18. <https://doi.org/10.3390/md18010035>

1011 Park, S.-H., Lee, K., Jang, J.W., Hahn, J.-S., 2019. Metabolic Engineering of *Saccharomyces*
1012 *cerevisiae* for Production of Shinorine, a Sunscreen Material, from Xylose. *ACS Synth Biol*
1013 8, 346–357. <https://doi.org/10.1021/acssynbio.8b00388>

1014 Perez-Riverol, Y., Bai, J., Bandla, C., García-Seisdedos, D., Hewapathirana, S.,
1015 Kamatchinathan, S., Kundu, D.J., Prakash, A., Frericks-Zipper, A., Eisenacher, M., Walzer,
1016 M., Wang, S., Brazma, A., Vizcaíno, J.A., 2022. The PRIDE database resources in 2022: a
1017 hub for mass spectrometry-based proteomics evidences. *Nucleic Acids Res* 50, D543–
1018 D552. <https://doi.org/10.1093/nar/gkab1038>

1019 Pope, M.A., Spence, E., Seralvo, V., Gacesa, R., Heidelberger, S., Weston, A.J., Dunlap, W.C.,
1020 Shick, J.M., Long, P.F., 2015. O-Methyltransferase Is Shared between the Pentose
1021 Phosphate and Shikimate Pathways and Is Essential for Mycosporine-Like Amino Acid
1022 Biosynthesis in *Anabaena variabilis* ATCC 29413. *ChemBioChem* 16, 320–327.
1023 <https://doi.org/https://doi.org/10.1002/cbic.201402516>

1024 Portwich, A., Garcia-Pichel, F., 2003. Biosynthetic pathway of mycosporines (mycosporine-like
1025 amino acids) in the cyanobacterium *Chlorogloeopsis* sp. strain PCC 6912. *Phycologia* 42,
1026 384–392. <https://doi.org/10.2216/i0031-8884-42-4-384.1>

1027 Qunjie, G., Ferran, G.-P., 2011. An ATP-Grasp Ligase Involved in the Last Biosynthetic Step of
1028 the Iminomycosporine Shinorine in *Nostoc punctiforme* ATCC 29133. *J Bacteriol* 193,
1029 5923–5928. <https://doi.org/10.1128/jb.05730-11>

1030 Rao, X., Li, D., Su, Z., Nomura, C.T., Chen, S., Wang, Q., 2024. A smart RBS library and its
1031 prediction model for robust and accurate fine-tuning of gene expression in *Bacillus* species.
1032 *Metab Eng* 81, 1–9. <https://doi.org/https://doi.org/10.1016/j.ymben.2023.11.002>

1033 Roberto, D., Lucia, B., Cinzia, C., Donato, G., Elisabetta, D., Paola, A., Lucedio, G., Antonio, P.,
1034 2008. Sunscreens Cause Coral Bleaching by Promoting Viral Infections. *Environ Health*
1035 *Perspect* 116, 441–447. <https://doi.org/10.1289/ehp.10966>

1036 Salis, H.M., 2011. Chapter two - The Ribosome Binding Site Calculator, in: Voigt, C. (Ed.),
1037 *Methods in Enzymology*. Academic Press, pp. 19–42.
1038 <https://doi.org/https://doi.org/10.1016/B978-0-12-385120-8.00002-4>

1039 Schultz, J.C., Mishra, S., Gaither, E., Mejia, A., Dinh, H., Maranas, C., Zhao, H., 2022.
1040 Metabolic engineering of *Rhodotorula toruloides* IFO0880 improves C16 and C18 fatty
1041 alcohol production from synthetic media. *Microb Cell Fact* 21, 26.
1042 <https://doi.org/10.1186/s12934-022-01750-3>

1043 Shetty, R.P., Endy, D., Knight, T.F., 2008. Engineering BioBrick vectors from BioBrick parts. *J*
1044 *Biol Eng* 2, 5. <https://doi.org/10.1186/1754-1611-2-5>

1045 Silva, J.C., Gorenstein, M. V, Li, G.-Z., Vissers, J.P.C., Geromanos, S.J., 2006. Absolute
1046 Quantification of Proteins by LCMSE: A Virtue of Parallel ms Acquisition *S. *Molecular &*
1047 *Cellular Proteomics* 5, 144–156. [https://doi.org/https://doi.org/10.1074/mcp.M500230-](https://doi.org/https://doi.org/10.1074/mcp.M500230-MCP200)
1048 [MCP200](https://doi.org/https://doi.org/10.1074/mcp.M500230-MCP200)

1049 Storch, M., Casini, A., Mackrow, B., Fleming, T., Trewhitt, H., Ellis, T., Baldwin, G.S., 2015.
1050 BASIC: A New Biopart Assembly Standard for Idempotent Cloning Provides Accurate,
1051 Single-Tier DNA Assembly for Synthetic Biology. *ACS Synth. Biol.* 4, 781.

1052 Suh, S.-S., Hwang, J., Park, M., Seo, H.H., Kim, H.-S., Lee, J.H., Moh, S.H., Lee, T.-K., 2014.
1053 Anti-Inflammation Activities of Mycosporine-Like Amino Acids (MAAs) in Response to UV
1054 Radiation Suggest Potential Anti-Skin Aging Activity. *Mar Drugs* 12, 5174–5187.
1055 <https://doi.org/10.3390/md12105174>

1056 Tao, L., Jackson, R.E., Cheng, Q., 2005. Directed evolution of copy number of a broad host
1057 range plasmid for metabolic engineering. *Metab Eng* 7, 10–17.
1058 <https://doi.org/https://doi.org/10.1016/j.ymben.2004.05.006>

1059 Teresa, del C., L., R.J., J., R.-H.J., Tobias, F., Uwe, S., Estrella, D., 2007. Convergent
1060 Peripheral Pathways Catalyze Initial Glucose Catabolism in *Pseudomonas putida*:
1061 Genomic and Flux Analysis. *J Bacteriol* 189, 5142–5152. [https://doi.org/10.1128/JB.00203-](https://doi.org/10.1128/JB.00203-07)
1062 [07](https://doi.org/10.1128/JB.00203-07)

1063 Tian, T., Kang, J.W., Kang, A., Lee, T.S., 2019. Redirecting Metabolic Flux via Combinatorial
1064 Multiplex CRISPRi-Mediated Repression for Isopentenol Production in *Escherichia coli*.
1065 *ACS Synth Biol* 8, 391–402. <https://doi.org/10.1021/acssynbio.8b00429>

1066 Tiso, T., Sabelhaus, P., Behrens, B., Wittgens, A., Rosenau, F., Hayen, H., Blank, L.M., 2016.
1067 Creating metabolic demand as an engineering strategy in *Pseudomonas putida* –
1068 Rhamnolipid synthesis as an example. *Metab Eng Commun* 3, 234–244.
1069 <https://doi.org/https://doi.org/10.1016/j.meteno.2016.08.002>

1070 Torres, P., Santos, J.P., Chow, F., Pena Ferreira, M.J., dos Santos, D.Y.A.C., 2018.
1071 Comparative analysis of in vitro antioxidant capacities of mycosporine-like amino acids
1072 (MAAs). *Algal Res* 34, 57–67. <https://doi.org/https://doi.org/10.1016/j.algal.2018.07.007>

1073 Tsuge, Y., Kawaguchi, H., Yamamoto, S., Nishigami, Y., Sota, M., Ogino, C., Kondo, A., 2018.
1074 Metabolic engineering of *Corynebacterium glutamicum* for production of sunscreen
1075 shinorine. *Biosci., Biotechnol., Biochem.* 82, 1252.

1076 Wada, N., Sakamoto, T., Matsugo, S., 2015. Mycosporine-Like Amino Acids and Their
1077 Derivatives as Natural Antioxidants. *Antioxidants* 4, 603–646.
1078 <https://doi.org/10.3390/antiox4030603>

1079 Wang, J., Jiang, T., Milligan, S., Zhang, J., Li, C., Yan, Y., 2022. Improving isoprenol production
1080 via systematic CRISPRi screening in engineered *Escherichia coli*. *Green Chemistry* 24,
1081 6955–6964. <https://doi.org/10.1039/D2GC02255A>

1082 Wang, X., Baidoo, E.E.K., Kakumanu, R., Xie, S., Mukhopadhyay, A., Lee, T.S., 2022.
1083 Engineering isoprenoids production in metabolically versatile microbial host *Pseudomonas*
1084 *putida*. *Biotechnology for Biofuels and Bioproducts* 15, 137. [https://doi.org/10.1186/s13068-](https://doi.org/10.1186/s13068-022-02235-6)
1085 [022-02235-6](https://doi.org/10.1186/s13068-022-02235-6)

1086 Wang, Yan, Horlamus, F., Henkel, M., Kovacic, F., Schläfle, S., Hausmann, R., Wittgens, A.,
1087 Rosenau, F., 2019. Growth of engineered *Pseudomonas putida* KT2440 on glucose,
1088 xylose, and arabinose: Hemicellulose hydrolysates and their major sugars as sustainable
1089 carbon sources. *GCB Bioenergy* 11, 249–259.
1090 <https://doi.org/https://doi.org/10.1111/gcbb.12590>

1091 Wang, Ying, Ling, C., Chen, Y., Jiang, X., Chen, G.-Q., 2019. Microbial engineering for easy
1092 downstream processing. *Biotechnol Adv* 37, 107365.
1093 <https://doi.org/https://doi.org/10.1016/j.biotechadv.2019.03.004>

1094 Wehrs, M., Gladden, J.M., Liu, Y., Platz, L., Prah, J.-P., Moon, J., Papa, G., Sundstrom, E.,
1095 Geiselman, G.M., Tanjore, D., Keasling, J.D., Pray, T.R., Simmons, B.A., Mukhopadhyay,
1096 A., 2019. Sustainable bioproduction of the blue pigment indigoidine: Expanding the range
1097 of heterologous products in *R. toruloides* to include non-ribosomal peptides. *Green*
1098 *Chemistry* 21, 3394–3406. <https://doi.org/10.1039/C9GC00920E>

1099 Wen, Z., Zhang, S., Odoh, C.K., Jin, M., Zhao, Z.K., 2020. *Rhodospiridium toruloides* - A
1100 potential red yeast chassis for lipids and beyond. *FEMS Yeast Res* 20, foaa038.
1101 <https://doi.org/10.1093/femsyr/foaa038>

1102 Wohlers, K., Wirtz, A., Reiter, A., Oldiges, M., Baumgart, M., Bott, M., 2021. Metabolic
1103 engineering of *Pseudomonas putida* for production of the natural sweetener 5-ketofructose
1104 from fructose or sucrose by periplasmic oxidation with a heterologous fructose
1105 dehydrogenase. *Microb Biotechnol* 14, 2592–2604.
1106 <https://doi.org/https://doi.org/10.1111/1751-7915.13913>

1107 Yang, G., Cozad, M.A., Holland, D.A., Zhang, Y., Luesch, H., Ding, Y., 2018. Photosynthetic
1108 Production of Sunscreen Shinorine Using an Engineered Cyanobacterium. *ACS Synth Biol*
1109 7, 664–671. <https://doi.org/10.1021/acssynbio.7b00397>

1110 Yunus, I.S., Anfelt, J., Sporre, E., Miao, R., Hudson, E.P., Jones, P.R., 2022. Synthetic
1111 metabolic pathways for conversion of CO₂ into secreted short-to medium-chain
1112 hydrocarbons using cyanobacteria. *Metab Eng* 72, 14–23.
1113 <https://doi.org/https://doi.org/10.1016/j.ymben.2022.01.017>

1114 Yunus, I.S., Jones, P.R., 2018. Photosynthesis-dependent biosynthesis of medium chain-length
1115 fatty acids and alcohols. *Metab Eng* 49. <https://doi.org/10.1016/j.ymben.2018.07.015>

1116 Yunus, I.S., Palma, A., Trudeau, D.L., Tawfik, D.S., Jones, P.R., 2020. Methanol-free
1117 biosynthesis of fatty acid methyl ester (FAME) in *Synechocystis* sp. PCC 6803. *Metab Eng*
1118 57, 217–227. <https://doi.org/https://doi.org/10.1016/j.ymben.2019.12.001>

1119 Zhao, D., Zhu, X., Zhou, H., Sun, N., Wang, T., Bi, C., Zhang, X., 2021. CRISPR-based
1120 metabolic pathway engineering. *Metab Eng* 63, 148–159.
1121 <https://doi.org/https://doi.org/10.1016/j.ymben.2020.10.004>
1122